Interleukin-13 Immune Gene Therapy Prevents CNS Inflammation and Demyelination via Alternative Activation of Microglia and Macrophages

Peer-reviewed author version

Guglielmetti, Caroline; Le Blon, Debbie; SANTERMANS, Eva; Salas-Perdomo, Angelica; Daans, Jasmijn; De Vocht, Nathalie; Shah, Disha; Hoornaert, Chloe; Praet, Jelle; Peerlings, Jurgen; Kara, Firat; Bigot, Christian; Mai, Zhenhua; Goossens, Herman; HENS, Niel; HENDRIX, Sven; Verhoye, Marleen; Planas, Anna M.; Berneman, Zwi; van der Linden, Annemie & Ponsaerts, Peter (2016) Interleukin-13 Immune Gene Therapy Prevents CNS Inflammation and Demyelination via Alternative Activation of Microglia and Macrophages. In: GLIA, 64(12), p. 2181-2200.

DOI: 10.1002/glia.23053
Handle: http://hdl.handle.net/1942/23036

Interleukin-13 immune gene therapy prevents CNS inflammation and demyelination via alternative activation of microglia and macrophages.

Caroline Guglielmetti[1], Debbie Le Blon[2,3], Eva Santermans[4], Angelica Salas-Perdomo[5], Jasmijn Daans[2,3], Nathalie De Vocht[1,2,3], Disha Shah[1], Chloé Hoornaert[2,3], Jelle Praet[1], Jurgen Peerlings[1], Firat Kara[1], Christian Bigot[1], Zhenhua Mai[1,6], Herman Goossens[3], Niel Hens[3,4,7], Sven Hendrix[8], Marleen Verhoye[1], Anna M. Planas[5], Zwi Berneman[2,3], Annemie van der Linden[1], Peter Ponsaerts[2,3]

[1] Bio-Imaging Laboratory, University of Antwerp, Antwerp, Belgium.

[2] Laboratory of Experimental Hematology, University of Antwerp, Antwerp, Belgium.

[3] Vaccine and Infectious Disease Institute (Vaxinfectio), University of Antwerp, Antwerp, Belgium.

[4] Center for Statistics, I-Biostat, Hasselt University, Hasselt, Belgium.

[5] Department of Brain Ischemia and Neurodegeneration, Institut d'Investigacions Biomèdiques de Barcelona (IIBB), Consejo Superior de Investigaciones Científicas (CSIC), Institut d'Investigacions Biomèdiques August Pi i Sunyer (IDIBAPS), Barcelona, Spain.

[6] Icometrix, Leuven, Belgium.

[7] Centre for Health Economic Research and Modelling Infectious Diseases (Chermid), University of Antwerp, Antwerp, Belgium.

[8] Department of Morphology, Biomedical Research Institute, Hasselt University, Diepenbeek, Belgium.

Running title:

Modulation of CNS inflammation by interkeukin-13

Corresponding author:

Prof. Dr. Peter Ponsaerts, Experimental Cell Transplantation Group, Laboratory of Experimental Hematology, Vaccine and Infectious Disease Institute (Vaxinfectio), University of Antwerp, Campus Drie Eiken (CDE-S6.51), Universiteitsplein 1, 2610 Antwerp (Wilrijk), Belgium.

Tel.: +32-3-2652428 - E-mail: peter.ponsaerts@uantwerpen.be

Exact number of words:

Abstract: 190 words

Text: 7755 words

Introduction (576 words), Materials and methods (2460 words), Results (2403 words), Discussion (2316 words)

Acknowledgements: 137 words

References: 2877 words

Figure legends: 1716 words

Number of figures: 8 figures

Supporting information: 382 words

Supporting table: 12 words; 1 supporting table

Supporting figures: 370 words; 3 supporting figures

Total word count: 13057 words (From abstract until figure legends, including supporting information)

Main points:

- Magnetic resonance imaging provides means to evaluate response to IL-13 therapy.
- IL-13 immune gene therapy protects against cuprizone-induced demyelination.
- IL-13 immune gene therapy induces alternative activation of microglia and macrophages.

Key words:

demyelination, multiple sclerosis, magnetic resonance imaging

ABSTRACT

Detrimental inflammatory responses in the central nervous system are a hallmark of various brain injuries and diseases. With this study we provide evidence that lentiviral vector-mediated expression of the immune-modulating cytokine interleukin 13 (IL-13) induces an alternative activation program in both microglia and macrophages conferring protection against severe oligodendrocyte loss and demyelination in the cuprizone mouse model for multiple sclerosis (MS). First, IL-13 mediated modulation of cuprizone-induced lesions was monitored using T_2-weighted magnetic resonance imaging and magnetization transfer imaging, and further correlated with quantitative histological analyses for inflammatory cell influx, oligodendrocyte death and demyelination. Second, following IL-13 immune gene therapy in cuprizone-treated $eGFP^+$ bone marrow chimeric mice, we provide evidence that IL-13 directs the polarization of both brain-resident microglia and infiltrating macrophages towards an alternatively activated phenotype, thereby promoting the conversion of a pro-inflammatory environment towards an anti-inflammatory environment, as further evidenced by gene expression analyses. Finally, we show that IL-13 immune gene therapy is also able to limit lesion severity in a pre-existing inflammatory environment. In conclusion, these results highlight the potential of IL-13 to modulate microglia/macrophage responses and to improve disease outcome in a mouse model for MS.

INTRODUCTION

While innate immune cells of the central nervous system (CNS) at one hand play a major role in development and maintenance of brain integrity and function (Kettenmann et al. 2011; Nimmerjahn et al. 2005; Ransohoff and Perry 2009), dysregulation of CNS immune responses on the other hand is highly associated with the pathophysiology of various neurodegenerative diseases (Perry et al. 2010; Prinz et al. 2011), including demyelinating disorders like multiple sclerosis (MS) (Lassmann and van Horssen 2016; Mahad et al. 2015; Rawji and Yong 2013; Sriram 2011). Microglia, well-recognized as brain tissue-specific macrophages (Chan et al. 2007; Ginhoux et al. 2010; Ginhoux et al. 2013; Tambuyzer et al. 2009), have the unique capacity to sense alterations of the brain microenvironment, and in response rapidly migrate, proliferate and undergo specific differentiation programs in order to restore brain homeostasis (Ousman and Kubes 2012). Functionally differentiated microglia and macrophages are commonly subdivided in two categories (Martinez and Gordon 2014; Mills et al. 2000; Mosser and Edwards 2008; Murray et al. 2014), the classically activated phenotype, which is characterized by the secretion of pro-inflammatory and cytotoxic mediators, and the alternatively activated phenotype, which generally contributes to extracellular matrix remodelling, progenitor cell differentiation and tissue regeneration. Experimental modulation of these microglia and macrophage polarization states can easily be achieved *in vitro* through supplementation of microglia/macrophage cultures with lipopolysaccharides (LPS) and interferon gamma (IFN-Ɣ) or with interleukin (IL)-4/13 to induce the classically activated or the alternatively activated polarization state, respectively (Gordon 2003; Mills et al. 2000). In this study, our main aim is to investigate whether targeted *in vivo* delivery of IL-13 at the onset of, or during neuro-inflammatory processes, can alter degenerative (histo-)pathological disease outcomes.

Activated microglia and macrophages are suggested to co-orchestrate oligodendrocyte death in the cuprizone mouse model of CNS demyelination (Hiremath et al. 1998; Kipp et al. 2009; Matsushima and

Morell 2001; Praet et al. 2014a). In this study we applied lentiviral vector (LV)-mediated transduction of the splenium of the corpus callosum (CC), i.e. the brain area affected most prominent in this neuro-inflammation mouse model, in order to investigate the effect of IL-13 on developing neuro-inflammatory lesions and subsequent demyelinating events. While recent *in vivo* treatment strategies aiming at directing the differentiation of microglia and macrophages towards an alternatively activated state highly rely on histological analyses to demonstrate reduced CNS damage and improved disease outcome (Hu et al. 2012; Ma et al. 2015; Miron et al. 2013; Yang et al. 2015), we here additionally performed magnetic resonance imaging (MRI) as the gold standard for *in vivo* detection of demyelinating lesions in CNS white matter (Polman et al. 2011; Trip and Miller 2005). In addition to standard T_2-weighted MRI, we also utilized magnetization transfer imaging (MTI) as an emerging technique to provide greater insight into the tissue microstructure in terms of inflammation, gliosis and myelination (Ropele and Fazekas 2009). Hence, we here report on multiparametric MRI approaches complementary and correlating to our quantitative histological analyses for an accurate *in vivo* monitoring of CNS inflammatory and demyelinating pathology, as well as the effect of IL-13 immune gene therapy thereon. Finally, as one of the major unsolved issues in CNS neuro-de/regeneration relates to the specific roles for CNS-resident microglia and CNS-invading peripheral macrophages (London et al. 2013), in our experimental setup using $eGFP^+$ bone marrow chimeric mice we attempted to clarify potential different and specific roles of both populations in disease and during IL-13 LV-mediated immune gene therapy in the CNS.

MATERIALS AND METHODS

Mice

C57BL/6J-*Tyr*$^{c\text{-}2J}$/J mice (albino C57BL/6J mice, strain code 000058) and transgenic C57BL/6-eGFP mice (strain code 003291) were obtained *via* Jackson Laboratories and bred in the animal facility of the University of Antwerp. For all experiments, mice were kept in normal day–night cycle (12/12) with *ad libitum* access to food and water. All experimental procedures were approved by the Ethics Committee for Animal Experiments of the University of Antwerp (Approval No 2011/13).

The cuprizone mouse model

At the age of eight weeks, mice received a standard rodent chow mixed with 0.2% w/w cuprizone (Sigma-Aldrich) for a period of 4 weeks in order to induce neuro-inflammation and CNS demyelination, as previously described (Guglielmetti et al. 2014; Orije et al. 2015; Praet et al. 2015a; Praet et al. 2012).

Lentiviral vector construction and production

The pCHMWS-IL-13-IRES-Pac lentiviral vector (LV) plasmid was constructed by replacing the eGFP cDNA insert (SpeI/XbaI digest) from the pCHMWS-eGFP-IRES-Pac plasmid (provided by the Leuven viral vector core, Molmed, KULeuven, Belgium) with the IL-13 cDNA (NcoI/NheI digest) from the pORF-mIL-13 plasmid (InvivoGen) using standard subcloning techniques(Hoornaert et al. 2016). The pCHMWS-BFP-IRES-Pac plasmid was constructed by replacing the eGFP cDNA insert (SpeI/XbaI digest) from the pCHMWS-eGFP-IRES-Pac plasmid with the BFP cDNA (SmaI/XbaI digest) from the TagBFP plasmid (Evrogen) (Le Blon et al. 2014). The pCHMWS-IL-4-IRES-Pac plasmid was constructed by replacing the eGFP cDNA insert (SpeI/XbaI digest) from the pCHMWS-eGFP-IRES-Pac plasmid with the IL-4 cDNA (NcoI/NheI digest) from the pORF-mIL-4 plasmid (InvivoGen). Before proceeding to LV production, all three plasmids were electroporated in K562 cells followed by stable selection by addition of puromycin to the culture medium. Expression of IL-13 or IL-4 was confirmed by a murine IL-13 or a murine IL-4

ELISA (Peprotech), respectively. Expression of the BFP reporter protein was confirmed by flow cytometric analysis. Following confirmation of IL-13, IL-4 and BFP expression, LV production was outsourced to the Leuven viral vector core, as previously described (Baekelandt et al. 2003; Geraerts et al. 2005).

Stereotaxic injections of lentiviral vector

All surgical interventions were performed according to institutional guidelines. Briefly, mice were anesthetized by intraperitoneal (IP) injection of a ketamine (75 mg/kg, Anesketin; Eurovet NV/SA) + medetomidine (1 mg/kg, Domitor; Pfizer Animal Health S.A.) mixture and positioned in a stereotactic head frame to achieve flat skull position (Stoelting). Stereotactic coordinates to target the splenium of the CC were as follows: AP -1.6 mm, Lat 0.3 mm and DV -1.1 mm (relative to bregma, Figure 1a). A midline scalp incision was made to expose the skull, and a hole was drilled in the skull using a dental drill burr (Stoelting). Thereafter, an automatic micro-injector pump (kdScientific) with a 10 µl Hamilton syringe was positioned above the exposed dura. A 32-gauge needle (Hamilton), attached to the syringe, was placed through the intact dura and positioned at the respective depth. After 2 min of pressure equilibration, 2 µl of LV concentrate ($1.5x10^7$-$3x10^7$ pg/ml p24) was injected at a speed of 0.5 µl/min. Before final needle retraction, a waiting period of 5 min was kept in order to allow for pressure equilibration and to prevent backflow of the injected LV suspension. Next, the skin was sutured (Vicryl, Ethicon) and a 0.9% NaCl (Baxter) solution was given subcutaneously in order to prevent dehydration while mice were placed under a heating lamp to recover. Anesthesia was reversed by an IP injection of atipamezol (Antisedan 5 mg/ml, Pfizer Animal Health S.A.).

Bone marrow transplantation

In order to discriminate microglia and macrophages, $eGFP^+$ bone marrow (BM) chimeric mice were generated as previously described (Le Blon et al. 2014). Briefly, four to six weeks old mice received 10Gy total body irradiation using an XRAD320 small animal irradiation device (Precision X-Ray). For

this, groups of five non-anesthetised mice were placed in a single cage within the whole irradiation field (without head protection). Next, a single intravenous injection of total $eGFP^+$ BM cells ($1.5x10^6$ cells in 100µl PBS) was administered via the tail vein within 6 hours post-irradiation. Total $eGFP^+$ BM cells were isolated from 8-week old C57BL/6-eGFP mice by flushing dissected femurs and tibias with sterile PBS. Before administration, total BM cells were filtered over a 70 µm sterile mesh (Becton Dickinson), centrifuged and suspended in PBS. During recovery, mice were treated with Enrofloxacin (1µl/mL; Baytril 10%; Bayer) added to the drinking water for 4 weeks post-irradiation.

Magnetic resonance imaging acquisition

In vivo imaging experiments were conducted at 400 MHz on a 9.4T Bruker Biospec system (Biospec 94/20 USR, Bruker Biospin) using a standard Bruker cross coil setup, with a quadrature volume coil for excitation and quadrature mouse surface coil for signal detection. During imaging, mice were anesthetized using 2% isoflurane (Isoflo®, Abbot Laboratories Ltd.) in a mixture of 30% O_2 and 70% N_2O at a flow rate of 600 ml/min. Mice were fixed in an animal restrainer with ear bars and a tooth bar. Respiratory rate was continuously monitored and body temperature was measured and maintained constant at 37°C using a feedback coupled warm air system (MR compatible Small Animal Monitoring and Gating System, SA instruments, Inc.). First, anatomical RARE-T_2 images were acquired to determine the position of the mouse in the magnet and enable a uniform position of the coronal slices for every T_2 and MTI experiments (repetition time (TR) = 2500 ms; echo time (TE [effective]) = 33.44 ms; RARE factor = 8; number of slices (NS) = 16 with a slice thickness of 0.4 mm; field of view (FOV) = 20 x 20 mm; matrix size = 256 x 256; in-plane resolution of 0.078 x 0.078 mm; scan time = 1 min 20 seconds). T_2 values were acquired with the Multi-Slice, Multi-Echo (MSME) sequence that is based on the Carr-Purcell-Meiboom-Gill (CPMG) sequence, where transverse magnetization of a 90° pulse is refocused by a train of 180° pulses generating a series of echoes. The following imaging parameters were used: number of averages (NA) = 1; NS= 6 with a slice thickness of 0.4 mm and an interslice thickness of 0.4 mm; number of echoes = 10 with echo spacing = 8.5 ms (TE) being 8.5; 17; 25.5; 34; 42.5; 51; 59.5; 68;

76.5; 85); TR = 4000 ms; FOV = 20 x 20 mm; matrix size = 256 x 256; in-plane resolution = 0.078 x 0.078 mm, scan time = 12 min 48 seconds). For magnetization transfer contrast (MTC) MRI, an off-resonance RF pulse was incorporated into a RARE T_2 sequence (TR = 4100 ms, TE [effective]= 33.44 ms; RARE factor = 8; NS = 1 with a slice thickness of 1 mm, FOV = 20 × 20 mm, matrix size = 192 × 192, in-plane resolution of 0.104 x 0.104 mm, NA = 3, scan time = 4 min 55 seconds). RARE T_2 images were acquired without off-resonance RF pulse (unsaturated) and with off-resonance RF pulse (saturated) applied (pulse strength = 3 µT; pulse length = 4000 ms, saturation time = 0.244 ms) at the offset frequency of 2000 Hz. MTC MRI was acquired at two different location of the mouse brain, first at the level of the splenium of the CC, and second at the level of the external capsule.

Magnetic resonance imaging processing

T_2 maps were generated with custom-built programs written in MATLAB (MATLAB R2011b, The MathWorks Inc.) using a monoexponential fit function [$y= A+C*\exp(-t/T_2)$], where A = Absolute bias, C = signal intensity, T_2 = transverse relaxation time. Regions of interest (ROIs) were drawn manually on the T_2-weighted images (Figure 1b), according to a mouse brain atlas, with AMIRA software (Mercury Computer systems) and regional average T_2 values were calculated. ROIs included the external capsule and the splenium of the CC. For MTI experiments, saturated images were realigned to the unsaturated image using AMIRA, for each animal separately. The realigned images were used to calculate magnetization transfer ratio (MTR) = (unsaturated − saturated) / unsaturated). ROIs were manually delineated on the MTR images (Figure 1b) and the mean MTR were calculated for the external capsule and the splenium of the CC.

Immunofluorescence analysis

All immunofluorescence analyses were performed according to previously described procedures (Praet et al. 2014b; Reekmans et al. 2013). Mice were first perfused with an ice cold 0.9% NaCl solution followed by an ice cold 4% paraformaldehyde (PFA) solution. Next, brains were dissected and further

fixated in 4% PFA for 2h, then dehydrated through a sucrose gradient (2h at 5%, 2h at 10% and overnight at 20%). Afterwards, brain tissue was snap-frozen in liquid nitrogen and kept at -80°C until further processing. Ten µm-thick cryosections were collected using a microm cryostat. Immunofluorescence staining was performed on brain slides using the following antibody combinations: a primary chicken anti-MBP antibody (Millipore, AB9348; 1:200 dilution) with a secondary donkey anti-chicken dylight 549 antibody (Jackson, 703-506-155, 1:1000 dilution); a primary rabbit anti-GFAP antibody (Abcam, ab7779, 1:500 dilution) with a secondary donkey anti-rabbit Alexa Fluor 555 antibody (Invitrogen, A31572, 1:1000 dilution); a mouse anti-APC/CC1 antibody (Calbiochem, OP80; 1:100 dilution) in combination with a goat anti-mouse Alexa Fluor 555 antibody (Invitrogen, AF21425; 1:1000 dilution); a primary rat anti-F4/80 antibody (AbD serotec, MCA497R, 1:250 dilution) with a secondary goat anti-rat Alexa Fluor 555 (Invitrogen, A21434, 1:200 dilution); a primary rabbit anti-Iba1 antibody (Wako, 01919741, 1:500 dilution) with a secondary donkey anti-rabbit AF555 (Invitrogen, A31572, 1:1000 dilution); a primary rat anti-mouse CD11b antibody (Immunotools, 22159111, 1:200 dilution) with a secondary goat anti-rat Alexa Fluor 555 (Invitrogen, A21434, 1:200 dilution); a primary rat anti-MHCII antibody (eBioscience, 14-5321-82, 1:200 dilution) with a secondary goat anti-rat Alexa Fluor 350 antibody (Invitrogen, A21093, 1:200 dilution); a primary rat anti-MHCII biotinylated antibody (eBioscience, 13-5321-85, 1:200 dilution) in combination with a streptavidin-Cy5 conjugate (Invitrogen, SA1011, 1:50 dilution); a primary goat anti-Arg-1 antibody (Santa Cruz, sc-18354, 1:50 dilution) with a secondary donkey anti-goat Alexa Fluor 555 (Invitrogen, A21432, 1:200 dilution) or donkey anti-goat Alexa Fluor 350 (Invitrogen, A21081, 1:200 dilution). Slides were counterstained using TOPRO-3 (Invitrogen, T3605, 1:200 dilution) or DAPI (Sigma, 1:1000 dilution). Following staining, sections were mounted using Prolong Gold Antifade (Invitrogen, P36930). Fluorescence image acquisition was performed using a standard research fluorescence microscope (Olympus Bx51 fluorescence microscope) equipped with an Olympus DP71 digital camera. Olympus cellSense Software (v 1.4) was used for wide field image acquisition.

Histological quantification

Quantitative analyses of macrophage and/or microglia responses were performed using TissueQuest immunofluorescence analysis software (TissueGnostics GmbH, v3.0), as previously described by us (De Vocht et al. 2013; Le Blon et al. 2014; Praet et al. 2015b; Reekmans et al. 2013). The following parameters were determined: the cellular density of F4/80$^+$ microglia/macrophages, the cellular density of Arg-1$^+$ microglia/macrophages, the cellular density of MHCII$^+$ microglia/macrophages and the cellular density of eGFP$^+$ macrophages, Additionally, the cellular density of CC-1$^+$ oligodendrocytes was determined using the same software. Using NIH ImageJ analysis software (v1.46r), the degree of glial fibrillary acidic protein (GFAP) astrogliosis and myelin basic protein (MBP) was determined based on the image-covering staining and expressed as percentage of the total area, as previously described by us (Praet et al. 2015a).

qRT-PCR

Mice were perfused with ice-cold 0.9% NaCl solution, directly followed by removal of the brain and dissection of the CC area around the injection site. The extracted tissue sections were immediately placed in RNALater solution (Ambion) and following overnight incubation at 4°C stored at -20°C until further processing. Total RNA was extracted using the Purelink RNA Kit (Invitrogen). RNA quantity and purity were determined using a ND-1000 micro-spectrophotometer (NanoDrop Technologies). One-µg total RNA was reverse-transcribed using a mixture of random primers (High Capacity cDNA Reverse Transcription kit, Applied Biosystems). PCR primers (provided in Supplementary Table S1) were designed with Primer3 software to bridge the exon–intron boundaries within the gene of interest to exclude amplification of contaminating genomic DNA. Primers were purchased from IDT (Laboratorios Conda S.A., Torrejon de Ardoz, Spain). Real-time quantitative RT-PCR analysis was carried out using SYBR green I dye detection (#11761500, Invitrogen) using the iCycler iQTM Multicolor Real-Time Detection System (Bio-Rad, Hercules, CA, USA). Optimized thermal cycling conditions were: 1 min at 50°C, 8 min and 30 sec at 95°C and 40 cycles of 15 sec at 95°C and 30 sec at 60°C. Data were collected

after each cycle and graphically displayed (iCycler iQTM Real-time Detection System Software, version 3.1, Bio-Rad). Melt curves were performed upon completion of the cycles to ensure specificity of the product amplification. Housekeeping gene for normalization was succinate dehydrogenase complex subunit A (SDHA). Data were analysed with the 2-ΔΔCT method. For comparison purposes, values of the samples of each group (n=8-10 mice per group) are expressed as fold versus the mean (n=7 mice) value of the control non-injected group.

Statistical analyses

Statistical analyses of the T_2 relaxation times and MTR were performed separately on the mean value of the splenium using (i) a one-way ANOVA for group comparison prior to cuprizone administration (W0) and (ii) using a (random effects) linear regression model for group comparison after four weeks of cuprizone administration, as described by the following equations:

$$\mathrm{Y}_1 = \Delta_{\mathrm{T}_2} = \mathrm{T2}_{\mathrm{W4}} - \mathrm{T2}_{\mathrm{W0}},$$

$$\mathrm{Y}_2 = \Delta_{\mathrm{MTR}} = \mathrm{MTR}_{\mathrm{W4}} - \mathrm{MTR}_{\mathrm{W0}}.$$

with Y_1 and Y_2 defined as the difference between the mean T_2 relaxation times or the mean MTR after four weeks of cuprizone administration (W4) and W0. For the EC, statistical analyses of the T_2 relaxation times and MTR were performed separately on the mean value of the left and right EC using a linear mixed model. The obtained p-values were corrected for multiple testing using the Tukey HSD post-hoc test.

For the results obtained from histological analyses the following statistical analyses were applied: (i) Comparison between experimental groups in cellular density for CC-1^+ cells and F4/80^+ cells as well as the coverage percentage of MBP and GFAP were analyzed using one-way ANOVA, and the given p-values were corrected for multiple testing using the Tukey HSD post-hoc test. (ii) The appearance of MHCII- and Arg1-expressing F4/80 cells was analyzed using one sample t test. (iii) Comparison between groups in cellular density of $eGFP^+$ macrophages were analyzed using generalized estimating equations (GEE), with the given p-values being corrected for multiple testing using the false discovery rate

method. (iv) The appearance of MHCII- and Arg1-expressing $eGFP^-$ microglia and $eGFP^+$ macrophages was analyzed using GEE, with the given p-values being corrected for multiple testing using the false discovery rate method. (iv) The dependence of MBP and GFAP coverage percentage, and cellular density for $CC\text{-}1^+$ and $F4/80^+$ between T_2 relaxation times or MTR was measured using the Spearman's correlation coefficient. Correlation coefficients and p-values are stated in the results section. For the results obtained with qRT-PCR, group comparison was performed using a Wilcoxon rank sum test with FDR correction. All of the above data and/or analyses are presented either in dot plots or in graphs showing mean ± standard deviation (SD) or standard error of the mean (SEM), as indicated in the figure legends. A p-value of <0.05 was considered statistically significant.

RESULTS

Non-invasive magnetic resonance imaging reveals less severe T_2 and MTR deviation in the splenium of cuprizone treated mice following IL-13 LV injection.

Before initiating therapeutic experiments, correct stereotactic targeting of the LV injections to the splenium was optimised using the BFP LV and validated by means of histological analysis (Figure 1a). In order to investigate the effect of IL-13 expression in the splenium on cuprizone induced inflammation and demyelination, non-injected control mice (No inj.), blue fluorescent protein (BFP) LV injected mice and IL-13 LV injected mice were randomly assigned to a subgroup that received a 4-week regular rodent diet (CONTROL) or a subgroup that received a 4-week cuprizone supplemented diet (CUPRIZONE) (Figure 2a). This 4-week time point was chosen as it corresponds to the optimal time window in the cuprizone mouse model comprising the highest level of microglia/macrophage activation with extensive demyelination in the splenium (Praet et al. 2014a). In this part of the study, non-invasive MRI was performed on all mice prior to LV injection and/or cuprizone administration and at the end of the 4-week study period. For analysis of MRI data, regions of interest were delineated on obtained T_2 and MTR maps at the level of the splenium (Figure 1b upper row). No significant differences in T_2 or MTR values were observed between the 6 different groups at the beginning of the experiment (data not shown). After 4 weeks, while non-injected mice, BFP LV injected mice and IL-13 LV injected mice that received a regular rodent diet displayed T_2 and MTR values comparable to baseline values (respectively Figures 2b + 2d and 2c + 2e, CONTROL No inj., BFP and IL-13), mice that received the cuprizone supplemented diet without LV injection or with injection of the BFP LV displayed significantly increased T_2 values and significantly decreased MTR values at the level of the splenium (respectively Figures 2b + 2d and 2c + 2e, CONTROL versus CUPRIZONE No inj. and BFP). These observations are suggestive for inflammation and demyelination in the splenium. Interestingly, cuprizone treated mice expressing IL-13 in the splenium displayed a significantly lower deviation of the normal T_2 and MTR values at the level of the splenium as compared to non-injected or BFP LV injected cuprizone treated

mice (Figures 2b + 2d and 2c + 2e, CUPRIZONE IL-13 versus CUPRIZONE No inj. and CUPRIZONE BFP). Lastly, we noted a strong inverse correlation between T_2 and MTR values (Figure 2f), implying that T_2 and MTR changes may be indicative of similar or associated pathological alterations. In summary, the presented data show that IL-13 immune gene therapy in the splenium strongly decreases cuprizone induced pathological alterations as assessed by non-invasive MRI measurements.

IL-13 LV injection in the splenium prevents cuprizone-induced inflammation, oligodendrocyte death and demyelination.

In order to further validate our imaging observations, quantitative histological analyses were performed. As expected, mice that received the cuprizone supplemented diet without LV injection or with injection of the BFP LV displayed a significantly lower number of CC-1^+ oligodendrocytes in the splenium, which further resulted in severe demyelination, as demonstrated by the significant loss of myelin basic protein (MBP) expression in the splenium (Figures 3a and 3b, CONTROL versus CUPRIZONE No inj. and CUPRIZONE BFP). Additionally, significant recruitment of F4/80^+ activated microglia/macrophages was observed in mice that received the cuprizone supplemented diet without LV injection or with injection of the BFP LV (Figures 3c, CONTROL versus CUPRIZONE No inj. and CUPRIZONE BFP). Similarly, significant astrocyte activation, as demonstrated GFAP$^+$ astrogliosis, was observed in mice that received the cuprizone supplemented diet without LV injection or with injection of the BFP LV (Figures 3d, CONTROL versus CUPRIZONE No inj. and CUPRIZONE BFP). In contrast, as already suggested by the MRI analyses, cuprizone treated mice expressing IL-13 in the splenium displayed significantly higher CC-1^+ oligodendrocyte numbers and less demyelination as compared to non-injected or BFP LV injected cuprizone treated mice (Figures 3a and 3b, CUPRIZONE IL-13 versus CUPRIZONE No inj. and CUPRIZONE BFP). Interestingly, cuprizone treated mice expressing IL-13 in the splenium also displayed significantly reduced recruitment of F4/80^+ activated microglia/macrophages (Figure 3c, CUPRIZONE IL-13 versus CUPRIZONE No inj. and CUPRIZONE BFP). In addition, also GFAP$^+$ astrogliosis was significantly decreased as compared to non-injected or BFP LV injected cuprizone

treated mice (Figure 3d, CUPRIZONE IL-13 versus CUPRIZONE No inj. and CUPRIZONE BFP). In agreement with our conclusion from the MRI analyses, histological data thus confirms that IL-13 LV injection in the splenium decreases cuprizone induced inflammatory responses and subsequent - at least in part - oligodendrocyte death and demyelination. Furthermore, given the large dataset obtained, we performed a correlation analysis between MRI metrics and histological metrics at the level of the splenium for all experimental groups. At one hand, Spearman correlation coefficients revealed an inverse correlation between T_2 values and the oligodendrocyte/myelin markers CC-1 and MBP (Supplementary Figure S1, $\rho = -0.8154$ and $\rho = -0.7997$, respectively) and a positive correlation between T_2 values and the inflammation-associated markers F4/80 and GFAP (Supplementary Figure S1, $\rho = 0.8506$ and $\rho = 0.7716$, respectively). On the other hand, MTR values display a positive correlation with the oligodendrocyte/myelin markers CC-1 and MBP (Supplementary Figure S1, $\rho = 0.7990$ and $\rho = 0.8318$, respectively) and an inverse correlation with the inflammation-associated markers F4/80 and GFAP (Supplementary Figure S1, $\rho = -0.8929$ and $\rho = -0.8229$, respectively). Concluding, and in agreement with preceding studies (Acs et al. 2009; Boretius et al. 2012; Chandran et al. 2012; Harsan et al. 2008; Thiessen et al. 2013; Torkildsen et al. 2009), both T_2 and MTR values can be used as predictive norms for monitoring cuprizone induces inflammatory and demyelinating events, including therapeutic intervention thereon.

IL-13 LV injection in the splenium protects locally during cuprizone-induced inflammation, oligodendrocyte death and demyelination.

Given the potential of IL-13 to interfere with the development of inflammatory and demyelinating events following cuprizone treatment, we additionally investigated whether the beneficial effect of IL-13 is restricted to the LV injection site (i.e. the splenium), or whether protection can be observed at cuprizone affected sites distinct from the splenium. For this, additional regions of interest were delineated on obtained T_2 and MTR maps in the external capsule at the level of the genu (Figure 1b, lower row). Here, all cuprizone treated mice display significantly increased T_2 values and significantly

decreased MTR values as compared to control groups indicating extensive demyelination and inflammation in the external capsule (Figures 4a and 4b, CONTROL versus CUPRIZONE). Interestingly, MTR, but not T_2 was able to detect a lower deviation of the normal MTR for mice that received the cuprizone diet and the IL-13 LV injection as compared to mice that received cuprizone and BFP LV injection or no injection (Figure 4b CUPRIZONE IL-13 versus CUPRIZONE No inj. and CUPRIZONE BFP). Further histological analyses, as shown by the representative images provided in figure 4, clearly showed a loss of CC-1^+ oligodendrocytes (Figure 4c), demyelination (Figure 4d), microglia/macrophage recruitment (Figure 4e) and astrogliosis (Figure 4f) at the level of the external capsule in cuprizone treated mice as compared to the control mice. Correlation analyses confirmed the findings reported for the splenium of the CC, i.e. an inverse correlation between T_2 and MTR ($\rho = -0.7666$, $p < 0.0001$) and similar association of MRI metrics with histological markers at the level of the external capsule (Supplementary Figure S2). Altogether these data suggest that expression of IL-13 in the splenium alters the response to cuprizone diet, but is not sufficient to rescue cuprizone-induced pathology in regions distinct from the LV injection site.

IL-13 LV injection in the splenium alters phenotypical properties of activated F4/80$^+$ microglia/macrophages during cuprizone treatment.

In order to further understand the observed protective effect of IL-13 LV injection in the splenium, we investigated the expression of major histocompatibility complex class II (MHCII) and Arginase-1 (Arg-1) by activated F4/80^+ microglia/macrophages. As already described above (Figure 3c), mice that received the cuprizone supplemented diet without LV injection displayed a significant increase of F4/80^+ microglia/macrophages at the level of the splenium compared to control mice (Figures 5a and 5b, CUPRIZONE No inj. versus CONTROL No inj., BFP LV and IL-13). Interestingly, a significant subpopulation of F4/80^+ activated microglia/macrophages in cuprizone treated mice displays MHCII expression upon BFP LV or IL-13 LV injection (Figure 5a, CUPRIZONE No inj. versus CUPRIZONE BFP and IL-13). Note that this subpopulation of MHCII$^+$ F4/80^+ activated microglia/macrophages also

significantly appears following BFP LV injection in control mice (Figure 5a, CONTROL BFP). Furthermore, a significant subpopulation of F4/80^{+} activated microglia/macrophages displays Arg-1 expression upon IL-13 LV injection only in cuprizone treated mice (Figure 5b CUPRIZONE IL-13 versus CUPRIZONE No inj. and BFP). Next, we investigated whether the observed F4/80+MHCII+ and F4/80+Arg-1+ cells are independent cell populations or whether they are the same cell population. Interestingly, upon co-staining of MHCII and Arg-1, it is clear that cuprizone treated mice expressing IL-13 present three distinct populations of cells which either are MHCII^{+}, Arg-1^{+} or Arg-1^{+}-MHCII^{+}, with the latter two being the most prominent (Figure 5c, CUPRIZONE IL-13). Summarizing, we here demonstrate that LV injection, either BFP LV or IL-13 LV, can modulate the activation state of F4/80^{+} activated microglia/macrophages as demonstrated by the expression of MHCII. Additionally, expression of IL-13 was able to induce Arg-1 expression in activated F4/80^{+} and F4/80^{+}MHCII^{+} microglia/macrophages, which might account for the beneficial effects observed on inflammation and demyelination.

IL-13 LV injection in the splenium induces a unique phenotype and cytokine profile during cuprizone treatment.

In order to further extend our hypothesis that IL-13 is capable of modulating inflammatory responses in cuprizone treated mice, we determined the mRNA expression levels of multiple cytokines and immune phenotype markers at the level of the CC in different experimental groups by means of qRT-PCR. At first, it is clear that mRNAs encoding Arg-1, YM-1 and Gal-3, which are associated with alternative microglia/macrophage activation, are significantly up-regulated in cuprizone treated mice injected with IL-13 LV, as compared to healthy control and non-injected cuprizone treated mice (Figures 6a, 6b and 6c). While the pro-inflammatory cytokines TNF-α, IL-1β and iNOS were significantly up-regulated in cuprizone treated mice injected with the BFP LV mice, but not in non-injected cuprizone treated mice, cuprizone treated mice injected with IL-13 LV were able to counteract TNF-α, but not IL-1β expression (Figures 6d, 6e and 6f). Unexpectedly, a small increase of iNOS mRNA was

detected in cuprizone treated mice injected with IL-13 LV (Figure 6f). Concluding, our results demonstrate that in vivo LV mediated IL-13 expression is capable to induce mRNA expression associated with alternative microglia/macrophage activation, which might lie at the basis of above-described inflammatory/neuro-protective effects in the cuprizone mouse model, but also indicates that LV mediated gene transfer on its own can shift neuro-inflammatory responses toward a more pro-inflammatory character. Nevertheless, downstream IL-13 events are capable - at least in part - to counteract LV mediated reinforcement of inflammatory responses.

Both microglia and macrophage phenotype is modulated through LV mediated expression of IL-13 in the splenium.

As the initiation and modulation of neuro-inflammation is a complex interplay between brain resident microglia and peripheral immune cells, we here investigated whether any of the observed $MHCII^+$, $Arg\text{-}1^+$ or $MHCII^+Arg\text{-}1^+$ cell populations can be specifically linked to microglia and/or macrophage cell populations. For this, we generated 8-week old $eGFP^+$ bone marrow chimeras that were subjected to BFP LV or IL-13 LV injection followed by 4 weeks of cuprizone administration. Non-injected cuprizone treated eGFP+ bone marrow chimeras served as control in this experimental setup (Figure 7a). Cuprizone-induced pathology and IL-13 LV protection was first verified by means of T_2-weighted imaging (Figure 7b). In agreement with the above-described results, $MHCII^+$ cells were detected in both BFP LV and IL-13 LV injected mice, while $Arg\text{-}1^+$ cells were only detected in IL-13 LV injected mice (Figure 7c, second + third column). Based on eGFP expression, which discriminates infiltrating $eGFP^+$ peripheral macrophages from brain resident $eGFP^-$ microglia, it can be noted that a significantly higher number of $eGFP^+$ peripheral macrophages contributes to - or at least are present - within cuprizone induced inflammatory lesions in the splenium upon BFP LV or IL-13 LV injection (Figure 7c, first column; Figure 7d, No inj. versus BFP and IL-13). Further co-localisation studies revealed that MHCII is expressed by both $eGFP^+$ macrophages and $eGFP^-$ microglia upon control BFP LV (Figure 7c, fourth column middle image; Figure 7e, BFP). Similarly - and highly interesting - co-localisation studies reveal that expression

of IL-13 in the splenium by means of LV injection and subsequent cuprizone administration leads to the significant appearance of 4 distinct inflammatory cell populations: $MHCII^+$, $Arg\text{-}1^+$ and $Arg\text{-}1^+MHCII^+$ $eGFP^+$ macrophages and $Arg\text{-}1^+MHCII^+$ $eGFP^-$ microglia (Figure 7c, fourth column lower image; Figure 7e, IL-13). These data indicate that both infiltrating macrophages and brain-resident microglia have the capacity to display Arg-1 expression in vivo upon stimulation with IL-13, and thereby potentially contribute to the beneficial effects observed on inflammation and demyelination.

Therapeutic LV mediated expression of IL-13 in the splenium protects against severe cuprizone-induced demyelination and is associated with an altered microglia/macrophages phenotype.

Finally, we further investigated whether IL-13 LV injection may also exert immunomodulatory and/or neuro-protective effects in a therapeutically relevant setup. For this, mice received a cuprizone supplemented diet for a period of 2.5 weeks in order to trigger a neuro-inflammatory response and oligodendrocyte metabolic impairment. After 2.5 weeks of cuprizone treatment, mice received an injection of the IL-13 LV and were kept under cuprizone diet for an additional 1.5 weeks, after which MRI evaluation and histological analyses were performed (Figure 8a). Although calculated T_2 values did not show a major difference between non-injected cuprizone treated mice and IL-13 LV injected mice, MTR values in contrast revealed a significantly lower deviation of the normal MTR in IL-13 LV injected cuprizone treated mice as compared to non-injected cuprizone treated mice, indicative for preservation of the splenium of the CC following IL-13 LV injection (Figures 8b and 8c). Subsequently, histological analyses (Figure 8d) confirmed a significant reduction $F4/80^+$ inflammatory cells (Figure 8e), with the remaining inflammatory cells being $Arg\text{-}1^+$ $MHC\text{-}II^{+/-}$ (Figure 8f). Furthermore, quantitative analysis of GFAP and MBP expression indicated significantly reduced astrogliosis and demyelination (Figures 8g and 8h). Most importantly, $CC1^+$ oligodendrocyte survival (Figure 8i) was significantly higher in the IL-13 LV injected CPZ group as compared to the non-injected CPZ control group. In summary, these results suggest that LV mediated expression of IL-13 can also be applied to a pre-existing neuro-

inflammatory environment in order to force microglia/macrophages into an alternative state of activation, with subsequent neuroprotective effects.

DISCUSSION

Halting the progression of brain damage while preventing and limiting further pathological alterations are critical steps for the treatment of progressive neurodegenerative diseases such as MS (Giunti et al. 2014; Goldmann and Prinz 2013; van Noort et al. 2011). In this study, we used the cuprizone mouse model of MS to induce highly inflammatory demyelinating lesions in the white matter (Gudi et al. 2014; Gudi et al. 2009; Orije et al. 2015; Remington et al. 2007; Steelman et al. 2012) and subsequently demonstrate that targeted delivery of IL-13 to the lesion site, prior and during lesion induction, induced the expression of markers characteristic for alternative activation both in microglia and macrophages. The latter is here shown to be associated with a protective effect on oligodendrocyte survival and subsequently less severe demyelination during cuprizone administration. These results are fully in line with current understandings of neuro-inflammatory processes in health and disease (Cherry et al. 2014; Murray et al. 2014; Rawji and Yong 2013), which suggest that modulating, rather than suppressing, microglial activation may be a more adequate therapeutic approach (David and Kroner 2011; Tang and Le 2016). Because microglia share functional similarities with peripheral macrophages, microglial activation and polarization state is generally classified using the established macrophage's nomenclature, i.e. classically activated, also referred as M1-like phenotype, or alternatively activated, also referred as M2-like phenotype, which in turn comprises several subtypes of cell activation (David and Kroner 2011; Hu et al. 2012). In the present study, we report on the *in vivo* induction of arginase1 expressing alternatively activated microglia and macrophages following LV mediated delivery of IL-13, similar to IL-4 a well described inducer of this specific subset of alternatively activated microglia and macrophages (Franco and Fernandez-Suarez 2015; Orihuela et al. 2016). Of note, although not described in detail in this manuscript, a similar set of experiments using an IL-4 encoding LV also demonstrates similar protection against demyelination upon injection into the splenium of cuprizone treated mice (Supplementary Figure S3). Following IL-13 LV administration, as well as following IL-4 LV administration, the alternatively activated state was associated with the prevention of the cuprizone-

induced pathology. The latter may not be unexpected as IL-4 and IL-13 share common receptor components (Kelly-Welch et al. 2003; Van Dyken and Locksley 2013), but may display divergent effects on microglia and macrophages. While macrophages generally are directed towards the M2 activation state (Dhakal et al. 2014; Murray et al. 2014; Orihuela et al. 2016), microglia may additionally be forced into apoptotic death under certain conditions following IL-4/13 stimulation (Won et al. 2013; Yang et al. 2002). At the time mentioned, we did not observe obvious differences between IL-13 and IL-4 mediated neuroprotection, and therefore decided to narrow down this study to the administration of IL-13, without specific preference.

In-situ delivery of compounds can be achieved through several means, including direct intracerebral injection of the molecule of interest (Kawahara et al. 2012), inoculation of nano-sized vehicles such as liposomes or nanoparticles containing the selected compound (Malam et al. 2009), direct engraftment of engineered cells producing the protein of interest (Stuckey and Shah 2014; Tan et al. 2005), or gene transfer using altered machinery of viruses (Houghton et al. 2015). Following our approach using LV injections in brains of healthy and cuprizone treated mice, several interesting observations were made. As observed on Figure 3, LV injections resulted in a slight activation of microglia and macrophages (Figure 3c, F4/80) and upregulation of MHCII expression in case of BFP LV injections in control mice (Figures 5a and 5c, MHCII), most likely illustrating the response to the viral particles and the attempt to eliminate them. Remarkably, in case of cuprizone administration, the vast majority of microglia and infiltrating macrophages at the level of the LV injection showed upregulation of MHCII, both in case of BFP or IL-13 LV injections (Figures 5, 7c, 7e and 8e), while only very little MHCII expression was observed in case of cuprizone treated mice that did not received a LV injection. These alterations in the pro-inflammatory phenotype following cuprizone administration in BFP LV injected animals was further confirmed by the significant upregulation of TNF-α mRNA (Figure 6d) and, albeit at a lower degree, the significant upregulation of IL-1β and iNOS mRNA (Figures 6e and 6f). As the latter qRT-PCR analyses were performed on the dissected splenium as a whole, we cannot distinguish whether the

detected TNF-α, IL-1β or iNOS mRNA transcripts were produced by microglia, macrophages or astrocytes. Nevertheless, these results are in line with previous studies showing that LV transduction can elicit a transient pro-inflammatory response against the LV particles (Kay 2011), mediated by the activation of toll-like receptor 7 and or toll-like receptor 9, which respectively recognize single stranded RNA and unmethylated CpG (Matrai et al. 2010). Consequently, the exacerbated immune response observed following cuprizone administration in BFP LV injected mice can be explained by a possible priming effect of innate immune cells following lentiviral vector infection and/or by the high infiltration of peripheral macrophages, caused by a blood brain barrier breakdown at the moment of the intracerebral surgery (Figure 7d), thereby modifying the lesion environment as compared to mice that did not received a LV injection (no mechanical blood-brain barrier damage and limited recruitment of peripheral macrophages). Likewise, we cannot exclude that priming of innate immune cells following lentiviral vector infection may be the key to successful IL-13 mediated deviation from classically activated towards alternatively activated microglia and macrophages, the latter upregulating, next to MHCII (Zurawski and de Vries 1994), also arginase1, YM-1 and galectin-3 (Figure 5b and 5c, Figure 6 a-c, Figure 7c and 7e, Figure 8e), which we associate with the beneficial effect on oligodendrocyte survival and myelin preservation. Interestingly, IL-13 was also able to counteract the upregulation of TNF-α mRNA as a consequence of LV injection. This is highly interesting in view of the observation that in TNF-α knock-out mice cuprizone administration results in a higher survival of oligodendrocytes and preservation of myelin up to 4 weeks after the start of the cuprizone diet (Arnett et al. 2001). Furthermore, our observations that IL-13 (and IL-4 immune gene therapy, Supplementary Figure S3) is able to exert beneficial effects on neuro-inflammation and demyelination in the cuprizone mouse model is also further supported by a recent publication by Janssens et al. showing that LV mediated delivery of oncostatin M (OSM) can induce alternatively activated microglia and macrophages via the upregulation of IL-4 expression, resulting in protection against cuprizone-induced demyelination (Janssens et al. 2015).

Clearly, induction of a phenotypic and/or functional state of alternative activation in microglia and macrophages is of high relevance in the process of inhibiting and/or modulating neuro-inflammation. However, to date it remains to be investigated in depth how IL-4/13 mediated alternative activation of microglia and macrophages displays protective features in vivo. In this context, we recently demonstrated that in vivo IL-13 priming of microglia and macrophages, with subsequent induction of F4/80, MHCII, arginase1, YM1 and Fizz1 expression, leads to highly reduced downstream effector function in terms of (i) direct in vivo recognition and elimination of allogeneic cellular grafts, and (ii) in vivo induction of allogeneic T-cell immune responses (Hoornaert et al. 2016). As such, it is clear that in vivo IL-13 primed microglia and macrophages display reduced and/or distinct effector functions as compared to pro-inflammatory microglia and/or macrophages phenotypes (in our studies defined as F4/80+ MHCII+ without expression of arginase1). Most widely suggested in literature is the competitive action of arginase1 with iNOS, thereby resulting in decreased NO production subsequently being less neurotoxic. Although this is certainly true for in vitro experiments in which microglia and macrophages can be primed towards the spectral ends of M1 and M2 activation by high concentrations of LPS/IFNg and IL-4/13, respectively, qRT-PCR experiments performed in this study (Figure 6) did not reveal significant iNOS expression in the CC of CPZ-treated mice in the absence of LV injection, thereby ruling out this mode-of-action in vivo for IL-13 mediated alternative activation of microglia and macrophages in the cuprizone model. Again this underscores our limited functional understanding of in vivo alternative activation of microglia and macrophages and warrants in depth in vitro and in vivo phenotypic and functional investigation of M1/M2 intermediate subtypes.

Although the main aim of this study was to investigate the influence of IL-13 immune gene therapy on inflammation and demyelination, several important aspects still remain to be elucidated. First, electron microscopy studies can provide additional information with regard to myelin integrity following IL-13 LV administration. Although not yet performed, we do not expect to observe normal myelin structure as still a significant degree of demyelination is present, as well as $CC1^{+}$

oligodendrocyte death as compared to healthy control mice. Secondly, further investigation should also reveal whether alternatively activated microglia and macrophages stimulated by the addition of IL-13 play a beneficial role in the repair process and remyelination once cuprizone administration is halted. While in our hands no classical M1- or M2-associated phenotypic markers can be found in the cuprizone model, a few studies have shown that microglia and macrophages display a distinct phenotype supportive of remyelination (Gudi et al. 2011; Morell et al. 1998; Olah et al. 2012; Voss et al. 2012). Along with the secretion of anti-inflammatory factors, growth factors and neurotrophic factors, there is accumulating evidence that phagocytosis of myelin debris is an essential step for a successful remyelination and that this step is ensured by alternatively activated polarized microglia and macrophages (Cantoni et al. 2015; Lampron et al. 2015; Poliani et al. 2015; Skripuletz et al. 2013). Furthermore, in the past years, numerous studies have reported the beneficial effect operated by the shift from M1- to M2-polarized immune cells in other preclinical models of MS and other models of neuro-inflammation (Cash et al. 1994; Janssens et al. 2015; Liu et al. 2013; Miro-Mur et al. 2016; Miron et al. 2013; Morganti et al. 2015; Ponomarev et al. 2007; Yu et al. 2015; Zhao et al. 2015). Specifically narrowing down on the distinct roles of microglia and macrophages in natural or therapeutic neuroprotection and/or repair, it will be of utmost importance to carefully design future studies allowing discrimination between both cell populations. Especially for the cuprizone mouse model, prior studies using bone marrow chimeric mice have reported that the population of monocyte-derived macrophages recruited to the corpus callosum following cuprizone administration represents 5 to 30% of the total number of microglia/macrophages (Lampron et al. 2015; Remington et al. 2007; Voss et al. 2012) in the absence of BBB disruption (Arnett et al. 2001; Matsushima and Morell 2001). Similarly, we used bone marrow chimeric mice to discern whether resident microglia and infiltrating monocyte-derived macrophages were equivalently affected by IL-13 stimulation and found that both populations displayed an alternatively activated phenotype (Figure 7c and 7e). Recently it has however been clearly shown that radiation bone marrow chimeric mice display an altered BBB permeability to systemic monocytes (Morganti et al. 2014), suggesting that certain results need caution during interpretation

as the function and recruitment of peripheral macrophages may slightly differ from non-irradiated non-injected animals. Nevertheless, our results were already able to demonstrate that IL-13 act on both microglia and infiltrating macrophages, while future experiments to be performed in the $CX3CR1^{eGFP/+}CCR2^{RFP/+}$ transgenic mouse model would surely help in further addressing these issues (Saederup et al. 2010).

Finally, we would like to elaborate a little further on our choice to non-invasively detect white matter lesions using multiparametric MRI. To date, MRI represents the method of choice for the evaluation and monitoring of demyelinating lesions over time in patients suffering from MS (Polman et al. 2011). We used T_2 relaxometry, a method routinely used in clinical settings (Poloni et al. 2011; Wattjes et al. 2015), in combination with a newly described method, magnetization transfer imaging that is sensitive to the integrity of macromolecules, notably myelin in the CNS (Grossman 1994; Ou et al. 2009; Turati et al. 2015). We demonstrated that both T_2 and MTR measures are highly correlated to the brain microstructure and underlying histopathological events following cuprizone administration (Supplementary Figures S1 and S2). Although a few studies have associated MTR values to oligodendrocytes numbers, myelin and GFAP positive astrocytes (Boretius et al. 2012; Fjaer et al. 2013; Merkler et al. 2005; Thiessen et al. 2013; Zaaraoui et al. 2008), we were unable to ascribe a specific MRI metric to a specific histological event. This is likely due to the fact that we used a four week cuprizone regime in which neuro-inflammation and demyelination are both reaching maximal values while other studies followed cuprizone induced changes over time, hence enabling to differentiate between sequential cellular events. Additionally, we here demonstrate that both T_2 and MTR measures are suitable to detect alterations in neuro-inflammation and associated demyelination following IL-13 LV therapeutic intervention. Moreover, we also show that MTI improved the detection of tissue alterations as compared to T_2, as MTI values reached significance when T_2 displayed a trend (Figures 4a + 4b and 8c + 8d), indicating a lower sensitivity threshold for MTI and highlighting its potential for future use in clinical practice. Moreover, by correlating T_2 and MTI measurements with quantitative

histological analyses, the multimodal character or this study clearly contributes to the validity of the observed therapeutic effect of IL-13 immune gene therapy.

In conclusion, the results presented in this study reveal a neuroprotective role of IL-13 in demyelinating lesions through the induction of alternatively activated microglia and macrophages. The ability of IL-13 to trigger the switch from a pro-inflammatory environment towards an anti-inflammatory environment, and thus limit CNS-induced pathology, is of particular interest for the design of new drug based therapies aiming at modulating microglial function to preserve tissue homeostasis and support remyelination in MS and other demyelinating diseases. In addition, these findings emphasize the beneficial action of alternatively activated immune cells that certainly deserve to be investigated in other pro-inflammatory-driven CNS pathological conditions, such as neurotrauma, spinal cord injury or stroke.

Acknowledgments:

This work was supported by research grants G.0136.11 (granted to PP, AVDL and ZB), G.0130.11 (granted to PP, AVDL and ZB) and G.0834.11 (granted to PP and SH) of the Fund for Scientific Research-Flanders (FWO-Vlaanderen, Belgium), in part by a Methusalem research grant from the Flemish government (granted to HG), in part by funding received from the European Union's Seventh Framework Programme (FP7/2007–2013) under grant agreement 278850 (INMiND) (granted to AVdL and AMP), in part by the Brainpath project (MSCA IAPP project granted to AVdL) and in part by funding received from the Belgian Charcot Foundation (granted to PP and AVdL). DLB, DS and CG hold a PhD-studentship from the Flemish Institute for Science and Technology (IWT-Vlaanderen). NDV and CH hold a PhD-studentship from the FWO-Vlaanderen. FK and JP hold a post-doctoral fellowship from the FWO-Vlaanderen.

References:

Acs P, Kipp M, Norkute A, Johann S, Clarner T, Braun A, Berente Z, Komoly S, Beyer C. 2009. 17beta-estradiol and progesterone prevent cuprizone provoked demyelination of corpus callosum in male mice. Glia 57:807-14.

Arnett HA, Mason J, Marino M, Suzuki K, Matsushima GK, Ting JP. 2001. TNF alpha promotes proliferation of oligodendrocyte progenitors and remyelination. Nat Neurosci 4:1116-22.

Baekelandt V, Eggermont K, Michiels M, Nuttin B, Debyser Z. 2003. Optimized lentiviral vector production and purification procedure prevents immune response after transduction of mouse brain. Gene Ther 10:1933-40.

Boretius S, Escher A, Dallenga T, Wrzos C, Tammer R, Bruck W, Nessler S, Frahm J, Stadelmann C. 2012. Assessment of lesion pathology in a new animal model of MS by multiparametric MRI and DTI. Neuroimage 59:2678-88.

Cantoni C, Bollman B, Licastro D, Xie M, Mikesell R, Schmidt R, Yuede CM, Galimberti D, Olivecrona G, Klein RS and others. 2015. TREM2 regulates microglial cell activation in response to demyelination in vivo. Acta Neuropathol 129:429-47.

Cash E, Minty A, Ferrara P, Caput D, Fradelizi D, Rott O. 1994. Macrophage-inactivating IL-13 suppresses experimental autoimmune encephalomyelitis in rats. J Immunol 153:4258-67.

Chan WY, Kohsaka S, Rezaie P. 2007. The origin and cell lineage of microglia: new concepts. Brain Res Rev 53:344-54.

Chandran P, Upadhyay J, Markosyan S, Lisowski A, Buck W, Chin CL, Fox G, Luo F, Day M. 2012. Magnetic resonance imaging and histological evidence for the blockade of cuprizone-induced demyelination in C57BL/6 mice. Neuroscience 202:446-53.

Cherry JD, Olschowka JA, O'Banion MK. 2014. Neuroinflammation and M2 microglia: the good, the bad, and the inflamed. J Neuroinflammation 11:98.

David S, Kroner A. 2011. Repertoire of microglial and macrophage responses after spinal cord injury. Nat Rev Neurosci 12:388-99.

De Vocht N, Lin D, Praet J, Hoornaert C, Reekmans K, Le Blon D, Daans J, Pauwels P, Goossens H, Hens N and others. 2013. Quantitative and phenotypic analysis of mesenchymal stromal cell graft survival and recognition by microglia and astrocytes in mouse brain. Immunobiology 218:696-705.

Dhakal M, Hardaway JC, Guloglu FB, Miller MM, Hoeman CM, Zaghouani AA, Wan X, Rowland LM, Cascio JA, Sherman MP and others. 2014. IL-13Ralpha1 is a surface marker for M2 macrophages influencing their differentiation and function. Eur J Immunol 44:842-55.

Fjaer S, Bo L, Lundervold A, Myhr KM, Pavlin T, Torkildsen O, Wergeland S. 2013. Deep gray matter demyelination detected by magnetization transfer ratio in the cuprizone model. PLoS One 8:e84162.

Franco R, Fernandez-Suarez D. 2015. Alternatively activated microglia and macrophages in the central nervous system. Prog Neurobiol 131:65-86.

Geraerts M, Michiels M, Baekelandt V, Debyser Z, Gijsbers R. 2005. Upscaling of lentiviral vector production by tangential flow filtration. J Gene Med 7:1299-310.

Ginhoux F, Greter M, Leboeuf M, Nandi S, See P, Gokhan S, Mehler MF, Conway SJ, Ng LG, Stanley ER and others. 2010. Fate mapping analysis reveals that adult microglia derive from primitive macrophages. Science 330:841-5.

Ginhoux F, Lim S, Hoeffel G, Low D, Huber T. 2013. Origin and differentiation of microglia. Front Cell Neurosci 7:45.

Giunti D, Parodi B, Cordano C, Uccelli A, Kerlero de Rosbo N. 2014. Can we switch microglia's phenotype to foster neuroprotection? Focus on multiple sclerosis. Immunology 141:328-39.

Goldmann T, Prinz M. 2013. Role of microglia in CNS autoimmunity. Clin Dev Immunol 2013:208093.

Gordon S. 2003. Alternative activation of macrophages. Nat Rev Immunol 3:23-35.

Grossman RI. 1994. Magnetization transfer in multiple sclerosis. Ann Neurol 36 Suppl:S97-9.

Gudi V, Gingele S, Skripuletz T, Stangel M. 2014. Glial response during cuprizone-induced de- and remyelination in the CNS: lessons learned. Front Cell Neurosci 8:73.

Gudi V, Moharregh-Khiabani D, Skripuletz T, Koutsoudaki PN, Kotsiari A, Skuljec J, Trebst C, Stangel M. 2009. Regional differences between grey and white matter in cuprizone induced demyelination. Brain Res 1283:127-38.

Gudi V, Skuljec J, Yildiz O, Frichert K, Skripuletz T, Moharregh-Khiabani D, Voss E, Wissel K, Wolter S, Stangel M. 2011. Spatial and temporal profiles of growth factor expression during CNS demyelination reveal the dynamics of repair priming. PLoS One 6:e22623.

Guglielmetti C, Praet J, Rangarajan JR, Vreys R, De Vocht N, Maes F, Verhoye M, Ponsaerts P, Van der Linden A. 2014. Multimodal imaging of subventricular zone neural stem/progenitor cells in the cuprizone mouse model reveals increased neurogenic potential for the olfactory bulb pathway, but no contribution to remyelination of the corpus callosum. Neuroimage 86:99-110.

Harsan LA, Steibel J, Zaremba A, Agin A, Sapin R, Poulet P, Guignard B, Parizel N, Grucker D, Boehm N and others. 2008. Recovery from chronic demyelination by thyroid hormone therapy: myelinogenesis induction and assessment by diffusion tensor magnetic resonance imaging. J Neurosci 28:14189-201.

Hiremath MM, Saito Y, Knapp GW, Ting JP, Suzuki K, Matsushima GK. 1998. Microglial/macrophage accumulation during cuprizone-induced demyelination in C57BL/6 mice. J Neuroimmunol 92:38-49.

Hoornaert CJ, Luyckx E, Reekmans K, Dhainaut M, Guglielmetti C, Le Blon D, Dooley D, Fransen E, Daans J, Verbeeck L and others. 2016. In Vivo Interleukin-13-Primed Macrophages Contribute to Reduced Alloantigen-Specific T Cell Activation and Prolong Immunological Survival of Allogeneic Mesenchymal Stem Cell Implants. Stem Cells.

Houghton BC, Booth C, Thrasher AJ. 2015. Lentivirus technologies for modulation of the immune system. Curr Opin Pharmacol 24:119-27.

Hu X, Li P, Guo Y, Wang H, Leak RK, Chen S, Gao Y, Chen J. 2012. Microglia/macrophage polarization dynamics reveal novel mechanism of injury expansion after focal cerebral ischemia. Stroke 43:3063-70.

Janssens K, Maheshwari A, Van den Haute C, Baekelandt V, Stinissen P, Hendriks JJ, Slaets H, Hellings N. 2015. Oncostatin M protects against demyelination by inducing a protective microglial phenotype. Glia 63:1729-37.

Kawahara K, Suenobu M, Yoshida A, Koga K, Hyodo A, Ohtsuka H, Kuniyasu A, Tamamaki N, Sugimoto Y, Nakayama H. 2012. Intracerebral microinjection of interleukin-4/interleukin-13 reduces beta-amyloid accumulation in the ipsilateral side and improves cognitive deficits in young amyloid precursor protein 23 mice. Neuroscience 207:243-60.

Kay MA. 2011. State-of-the-art gene-based therapies: the road ahead. Nat Rev Genet 12:316-28.

Kelly-Welch AE, Hanson EM, Boothby MR, Keegan AD. 2003. Interleukin-4 and interleukin-13 signaling connections maps. Science 300:1527-8.

Kettenmann H, Hanisch UK, Noda M, Verkhratsky A. 2011. Physiology of microglia. Physiol Rev 91:461-553.

Kipp M, Clarner T, Dang J, Copray S, Beyer C. 2009. The cuprizone animal model: new insights into an old story. Acta Neuropathol 118:723-36.

Lampron A, Larochelle A, Laflamme N, Prefontaine P, Plante MM, Sanchez MG, Yong VW, Stys PK, Tremblay ME, Rivest S. 2015. Inefficient clearance of myelin debris by microglia impairs remyelinating processes. J Exp Med 212:481-95.

Lassmann H, van Horssen J. 2016. Oxidative stress and its impact on neurons and glia in multiple sclerosis lesions. Biochim Biophys Acta 1862:506-10.

Le Blon D, Hoornaert C, Daans J, Santermans E, Hens N, Goossens H, Berneman Z, Ponsaerts P. 2014. Distinct spatial distribution of microglia and macrophages following mesenchymal stem cell implantation in mouse brain. Immunol Cell Biol 92:650-8.

Liu C, Li Y, Yu J, Feng L, Hou S, Liu Y, Guo M, Xie Y, Meng J, Zhang H and others. 2013. Targeting the shift from M1 to M2 macrophages in experimental autoimmune encephalomyelitis mice treated with fasudil. PLoS One 8:e54841.

London A, Cohen M, Schwartz M. 2013. Microglia and monocyte-derived macrophages: functionally distinct populations that act in concert in CNS plasticity and repair. Front Cell Neurosci 7:34.

Ma SF, Chen YJ, Zhang JX, Shen L, Wang R, Zhou JS, Hu JG, Lu HZ. 2015. Adoptive transfer of M2 macrophages promotes locomotor recovery in adult rats after spinal cord injury. Brain Behav Immun 45:157-70.

Mahad DH, Trapp BD, Lassmann H. 2015. Pathological mechanisms in progressive multiple sclerosis. Lancet Neurol 14:183-93.

Malam Y, Loizidou M, Seifalian AM. 2009. Liposomes and nanoparticles: nanosized vehicles for drug delivery in cancer. Trends Pharmacol Sci 30:592-9.

Martinez FO, Gordon S. 2014. The M1 and M2 paradigm of macrophage activation: time for reassessment. F1000Prime Rep 6:13.

Matrai J, Chuah MK, VandenDriessche T. 2010. Recent advances in lentiviral vector development and applications. Mol Ther 18:477-90.

Matsushima GK, Morell P. 2001. The neurotoxicant, cuprizone, as a model to study demyelination and remyelination in the central nervous system. Brain Pathol 11:107-16.

Merkler D, Boretius S, Stadelmann C, Ernsting T, Michaelis T, Frahm J, Bruck W. 2005. Multicontrast MRI of remyelination in the central nervous system. NMR Biomed 18:395-403.

Mills CD, Kincaid K, Alt JM, Heilman MJ, Hill AM. 2000. M-1/M-2 macrophages and the Th1/Th2 paradigm. J Immunol 164:6166-73.

Miro-Mur F, Perez-de-Puig I, Ferrer-Ferrer M, Urra X, Justicia C, Chamorro A, Planas AM. 2016. Immature monocytes recruited to the ischemic mouse brain differentiate into macrophages with features of alternative activation. Brain Behav Immun 53:18-33.

Miron VE, Boyd A, Zhao JW, Yuen TJ, Ruckh JM, Shadrach JL, van Wijngaarden P, Wagers AJ, Williams A, Franklin RJ and others. 2013. M2 microglia and macrophages drive oligodendrocyte differentiation during CNS remyelination. Nat Neurosci 16:1211-8.

Morell P, Barrett CV, Mason JL, Toews AD, Hostettler JD, Knapp GW, Matsushima GK. 1998. Gene expression in brain during cuprizone-induced demyelination and remyelination. Mol Cell Neurosci 12:220-7.

Morganti JM, Jopson TD, Liu S, Gupta N, Rosi S. 2014. Cranial irradiation alters the brain's microenvironment and permits CCR2+ macrophage infiltration. PLoS One 9:e93650.

Morganti JM, Jopson TD, Liu S, Riparip LK, Guandique CK, Gupta N, Ferguson AR, Rosi S. 2015. CCR2 antagonism alters brain macrophage polarization and ameliorates cognitive dysfunction induced by traumatic brain injury. J Neurosci 35:748-60.

Mosser DM, Edwards JP. 2008. Exploring the full spectrum of macrophage activation. Nat Rev Immunol 8:958-69.

Murray PJ, Allen JE, Biswas SK, Fisher EA, Gilroy DW, Goerdt S, Gordon S, Hamilton JA, Ivashkiv LB, Lawrence T and others. 2014. Macrophage activation and polarization: nomenclature and experimental guidelines. Immunity 41:14-20.

Nimmerjahn A, Kirchhoff F, Helmchen F. 2005. Resting microglial cells are highly dynamic surveillants of brain parenchyma in vivo. Science 308:1314-8.

Olah M, Amor S, Brouwer N, Vinet J, Eggen B, Biber K, Boddeke HW. 2012. Identification of a microglia phenotype supportive of remyelination. Glia 60:306-21.

Orihuela R, McPherson CA, Harry GJ. 2016. Microglial M1/M2 polarization and metabolic states. Br J Pharmacol 173:649-65.

Orije J, Kara F, Guglielmetti C, Praet J, Van der Linden A, Ponsaerts P, Verhoye M. 2015. Longitudinal monitoring of metabolic alterations in cuprizone mouse model of multiple sclerosis using 1H-magnetic resonance spectroscopy. Neuroimage 114:128-35.

Ou X, Sun SW, Liang HF, Song SK, Gochberg DF. 2009. The MT pool size ratio and the DTI radial diffusivity may reflect the myelination in shiverer and control mice. NMR Biomed 22:480-7.

Ousman SS, Kubes P. 2012. Immune surveillance in the central nervous system. Nat Neurosci 15:1096-101.

Perry VH, Nicoll JA, Holmes C. 2010. Microglia in neurodegenerative disease. Nat Rev Neurol 6:193-201.

Poliani PL, Wang Y, Fontana E, Robinette ML, Yamanishi Y, Gilfillan S, Colonna M. 2015. TREM2 sustains microglial expansion during aging and response to demyelination. J Clin Invest 125:2161-70.

Polman CH, Reingold SC, Banwell B, Clanet M, Cohen JA, Filippi M, Fujihara K, Havrdova E, Hutchinson M, Kappos L and others. 2011. Diagnostic criteria for multiple sclerosis: 2010 revisions to the McDonald criteria. Ann Neurol 69:292-302.

Poloni G, Minagar A, Haacke EM, Zivadinov R. 2011. Recent developments in imaging of multiple sclerosis. Neurologist 17:185-204.

Ponomarev ED, Maresz K, Tan Y, Dittel BN. 2007. CNS-derived interleukin-4 is essential for the regulation of autoimmune inflammation and induces a state of alternative activation in microglial cells. J Neurosci 27:10714-21.

Praet J, Guglielmetti C, Berneman Z, Van der Linden A, Ponsaerts P. 2014a. Cellular and molecular neuropathology of the cuprizone mouse model: clinical relevance for multiple sclerosis. Neurosci Biobehav Rev 47:485-505.

Praet J, Orije J, Kara F, Guglielmetti C, Santermans E, Daans J, Hens N, Verhoye M, Berneman Z, Ponsaerts P and others. 2015a. Cuprizone-induced demyelination and demyelination-associated inflammation result in different proton magnetic resonance metabolite spectra. NMR Biomed 28:505-13.

Praet J, Reekmans K, Lin D, De Vocht N, Bergwerf I, Tambuyzer B, Daans J, Hens N, Goossens H, Pauwels P and others. 2012. Cell type-associated differences in migration, survival, and immunogenicity following grafting in CNS tissue. Cell Transplant 21:1867-81.

Praet J, Santermans E, Daans J, Le Blon D, Hoornaert C, Goossens H, Hens N, Van der Linden A, Berneman Z, Ponsaerts P. 2015b. Early Inflammatory Responses Following Cell Grafting in the CNS Trigger Activation of the Subventricular Zone: A Proposed Model of Sequential Cellular Events. Cell Transplant 24:1481-92.

Praet J, Santermans E, Reekmans K, de Vocht N, Le Blon D, Hoornaert C, Daans J, Goossens H, Berneman Z, Hens N and others. 2014b. Histological characterization and quantification of cellular events following neural and fibroblast(-like) stem cell grafting in healthy and demyelinated CNS tissue. Methods Mol Biol 1213:265-83.

Prinz M, Priller J, Sisodia SS, Ransohoff RM. 2011. Heterogeneity of CNS myeloid cells and their roles in neurodegeneration. Nat Neurosci 14:1227-35.

Ransohoff RM, Perry VH. 2009. Microglial physiology: unique stimuli, specialized responses. Annu Rev Immunol 27:119-45.

Rawji KS, Yong VW. 2013. The benefits and detriments of macrophages/microglia in models of multiple sclerosis. Clin Dev Immunol 2013:948976.

Reekmans K, De Vocht N, Praet J, Le Blon D, Hoornaert C, Daans J, Van der Linden A, Berneman Z, Ponsaerts P. 2013. Quantitative evaluation of stem cell grafting in the central nervous system of mice by in vivo bioluminescence imaging and postmortem multicolor histological analysis. Methods Mol Biol 1052:125-41.

Remington LT, Babcock AA, Zehntner SP, Owens T. 2007. Microglial recruitment, activation, and proliferation in response to primary demyelination. Am J Pathol 170:1713-24.

Ropele S, Fazekas F. 2009. Magnetization transfer MR imaging in multiple sclerosis. Neuroimaging Clin N Am 19:27-36.

Saederup N, Cardona AE, Croft K, Mizutani M, Cotleur AC, Tsou CL, Ransohoff RM, Charo IF. 2010. Selective chemokine receptor usage by central nervous system myeloid cells in CCR2-red fluorescent protein knock-in mice. PLoS One 5:e13693.

Skripuletz T, Hackstette D, Bauer K, Gudi V, Pul R, Voss E, Berger K, Kipp M, Baumgartner W, Stangel M. 2013. Astrocytes regulate myelin clearance through recruitment of microglia during cuprizone-induced demyelination. Brain 136:147-67.

Sriram S. 2011. Role of glial cells in innate immunity and their role in CNS demyelination. J Neuroimmunol 239:13-20.

Steelman AJ, Thompson JP, Li J. 2012. Demyelination and remyelination in anatomically distinct regions of the corpus callosum following cuprizone intoxication. Neurosci Res 72:32-42.

Stuckey DW, Shah K. 2014. Stem cell-based therapies for cancer treatment: separating hope from hype. Nat Rev Cancer 14:683-91.

Tambuyzer BR, Ponsaerts P, Nouwen EJ. 2009. Microglia: gatekeepers of central nervous system immunology. J Leukoc Biol 85:352-70.

Tan PH, Beutelspacher SC, Xue SA, Wang YH, Mitchell P, McAlister JC, Larkin DF, McClure MO, Stauss HJ, Ritter MA and others. 2005. Modulation of human dendritic-cell function following transduction with viral vectors: implications for gene therapy. Blood 105:3824-32.

Tang Y, Le W. 2016. Differential Roles of M1 and M2 Microglia in Neurodegenerative Diseases. Mol Neurobiol 53:1181-94.

Thiessen JD, Zhang Y, Zhang H, Wang L, Buist R, Del Bigio MR, Kong J, Li XM, Martin M. 2013. Quantitative MRI and ultrastructural examination of the cuprizone mouse model of demyelination. NMR Biomed 26:1562-81.

Torkildsen O, Brunborg LA, Thorsen F, Mork SJ, Stangel M, Myhr KM, Bo L. 2009. Effects of dietary intervention on MRI activity, de- and remyelination in the cuprizone model for demyelination. Exp Neurol 215:160-6.

Trip SA, Miller DH. 2005. Imaging in multiple sclerosis. J Neurol Neurosurg Psychiatry 76 Suppl 3:iii11-iii18.

Turati L, Moscatelli M, Mastropietro A, Dowell NG, Zucca I, Erbetta A, Cordiglieri C, Brenna G, Bianchi B, Mantegazza R and others. 2015. In vivo quantitative magnetization transfer imaging correlates with histology during de- and remyelination in cuprizone-treated mice. NMR Biomed 28:327-37.

Van Dyken SJ, Locksley RM. 2013. Interleukin-4- and interleukin-13-mediated alternatively activated macrophages: roles in homeostasis and disease. Annu Rev Immunol 31:317-43.

van Noort JM, van den Elsen PJ, van Horssen J, Geurts JJ, van der Valk P, Amor S. 2011. Preactive multiple sclerosis lesions offer novel clues for neuroprotective therapeutic strategies. CNS Neurol Disord Drug Targets 10:68-81.

Voss EV, Skuljec J, Gudi V, Skripuletz T, Pul R, Trebst C, Stangel M. 2012. Characterisation of microglia during de- and remyelination: can they create a repair promoting environment? Neurobiol Dis 45:519-28.

Wattjes MP, Steenwijk MD, Stangel M. 2015. MRI in the Diagnosis and Monitoring of Multiple Sclerosis: An Update. Clin Neuroradiol 25 Suppl 2:157-65.

Won SY, Kim SR, Maeng S, Jin BK. 2013. Interleukin-13/Interleukin-4-induced oxidative stress contributes to death of prothrombinkringle-2 (pKr-2)-activated microglia. J Neuroimmunol 265:36-42.

Yang MS, Park EJ, Sohn S, Kwon HJ, Shin WH, Pyo HK, Jin B, Choi KS, Jou I, Joe EH. 2002. Interleukin-13 and -4 induce death of activated microglia. Glia 38:273-80.

Yang Y, Salayandia VM, Thompson JF, Yang LY, Estrada EY, Yang Y. 2015. Attenuation of acute stroke injury in rat brain by minocycline promotes blood-brain barrier remodeling and alternative microglia/macrophage activation during recovery. J Neuroinflammation 12:26.

Yu Z, Sun D, Feng J, Tan W, Fang X, Zhao M, Zhao X, Pu Y, Huang A, Xiang Z and others. 2015. MSX3 Switches Microglia Polarization and Protects from Inflammation-Induced Demyelination. J Neurosci 35:6350-65.

Zaaraoui W, Deloire M, Merle M, Girard C, Raffard G, Biran M, Inglese M, Petry KG, Gonen O, Brochet B and others. 2008. Monitoring demyelination and remyelination by magnetization transfer imaging in the mouse brain at 9.4 T. MAGMA 21:357-62.

Zhao X, Wang H, Sun G, Zhang J, Edwards NJ, Aronowski J. 2015. Neuronal Interleukin-4 as a Modulator of Microglial Pathways and Ischemic Brain Damage. J Neurosci 35:11281-91.

Zurawski G, de Vries JE. 1994. Interleukin 13, an interleukin 4-like cytokine that acts on monocytes and B cells, but not on T cells. Immunol Today 15:19-26.

FIGURE LEGENDS

Figure 1: Stereotaxic injection and MRI delineations.

(a) Coordinates for stereotaxic injections of LV at the level of the splenium of the CC. A representative direct immunofluorescence image of blue fluorescent protein (BFP) LV injected mice indicates stable expression of the transgene in the splenium up to four weeks post LV-injection. **(b)** Representative images of a control mouse indicating in red the delineations of the two regions of interest, i.e. the splenium and the external capsule on a T_2 map and MTR image.

Figure 2: Non-invasive magnetic resonance imaging reveals less severe T_2 and MTR deviation in the splenium of cuprizone treated mice following LV mediated expression of IL-13.

(a) To induce inflammation and demyelination, mice were fed a cuprizone supplemented diet for a period of four weeks, while mice of the control groups were fed a regular rodent chow. On the first day of cuprizone administration mice received an injection of a BFP LV or IL-13 LV or no injection (No inj.) and were assigned to a cuprizone or control group. MRI was performed prior to LV injection and after four weeks of cuprizone feeding, immediately followed by histological analysis. (b) Panel shows a representative T_2 map for each experimental group at the level of the splenium of the CC. Hyper-intense contrast can be visualized at the level of the splenium after cuprizone administration, reflecting inflammation and/or demyelination, but not for mice that also received the IL-13 LV injection (white arrows indicate the location of the CC of cuprizone treated mice). Scale bar = 1 mm. (c) In a similar manner, panel shows a representative color-coded MTR image for each experimental group at the level of the splenium of the CC. Disappearance of the CC (color-coded in red) can be observed after cuprizone administration, indicating inflammation and demyelination, but not for mice that also received the IL-13 LV injection (white arrows indicate the location of the CC of cuprizone treated mice). Scale bar = 1 mm. (d) T_2 values of individual mice are displayed in the graph with mean ± SD and reveal a lower deviation of the normal T_2 of IL-13 LV injected cuprizone treated mice (n = 5 - 14 mice).

*P<0.05, Linear regression model, Tukey post hoc test. (e) Similarly, MTR of individuals are displayed in the graph with mean ± SD and indicate a lower deviation of the MTR of IL-13 LV injected cuprizone treated mice (n = 5 - 14 mice). (f) Graph showing a strong inverse correlation between T_2 values and MTR. *P<0.05, ***P<0.001, Linear regression model, Tukey post hoc test.

Figure 3: LV mediated expression of IL-13 in the splenium prevents cuprizone-induced inflammation, oligodendrocyte death and demyelination.

Histological analyses performed at the level of the splenium for $CC1^+$ oligodendrocytes, MBP myelination, $F4/80^+$ activated microglia/macrophages and $GFAP^+$ astrogliosis are depicted in panels a, b, c and d, respectively, and confirm decreased oligodendrocyte cell loss and demyelination associated with a decreased microgliosis and astrogliosis in IL-13 LV injected cuprizone treated mice. *P<0.05, **P<0.01, ***P<0.001, One-way ANOVA and Tukey post hoc test (n = 3 - 6 mice). Scale bar = 100 µm.

Figure 4: LV mediated expression of IL-13 in the splenium protects locally against cuprizone-induced inflammation, oligodendrocyte death and demyelination.

Panel a shows a representative T_2 map for each experimental group at the level of the external capsule. Hyper-intense contrast can be visualized at the level of the external capsule, reflecting inflammation and/or demyelination. Scale bar = 1 mm. T_2 values of individual mice are displayed in the graph with mean± SD and reveal an increase of T_2 value in all cuprizone treated mice at the level of the external capsule (n = 5-14 mice). ***P<0.001, Linear mixed model , Tukey post hoc test. In a similar manner, panel b shows a representative color-coded MTR image for each experimental group at the level of the external capsule. Disappearance of the contrast from the external capsule (color-coded with red) can be visualized in groups that received the cuprizone supplemented diet, reflecting inflammation and/or demyelination. Scale bar = 1 mm. MTR of individual mice are displayed in the graph with mean ± SD and indicated a decrease of MTR in all cuprizone treated mice. *P<0.05, ***P<0.001, Linear regression model, Tukey post hoc test. (n = 5-11 mice). Histological analyses performed at the level of the external

capsule for $CC1^+$ oligodendrocytes, MBP myelination, $F4/80^+$ activated microglia/macrophages and $GFAP^+$ astrogliosis are depicted in panels c, d, e and f, respectively, and confirm oligodendrocytes cell loss and demyelination associated with the presence of microgliosis and astrogliosis and in all cuprizone treated mice at the level of the external capsule, independently of LV injection (n = 3-5 mice). Scale bar = 100 µm.

Figure 5: LV mediated expression of IL-13 in the splenium alters phenotypic properties of activated $F4/80^+$ microglia/macrophages during cuprizone treatment.

Phenotypic properties of microglia/macrophages at the level of the splenium of the CC was assessed after injection of LV followed by four weeks of cuprizone administration. (a) Representative images of each experimental group stained for F4/80 (red) and MHC-II (green). Scale bar =100 µm. Graph displays MHCII staining expressed as percentage relative of $F4/80^+$ cells of non-injected cuprizone treated mice ± SEM. Downward error bars for white coded bars. Upward error bars for black coded bars. Significant appearance of MHCII expression is indicated by the * sign. **P<0.01, ***P<0.001, One sample t-test (n= 3-6 mice). (b) Representative images of each experimental group stained for F4/80 (red) and Arg-1 (green). Scale bar =100 µm. Graph displays Arg-1 staining expressed as percentage relative of $F4/80^+$ cells of non-injected cuprizone treated mice ± SEM. Downward error bars for white coded bars. Upward error bars for black coded bars. Significant appearance of Arg-1 expression is indicated by the # sign. #P<0.05, One sample t-test (n= 3-6 mice). (c) Representative images of each experimental group stained for Arg-1 (red) and MHCII (green). Scale bar =100 µm. Graph shows the density of $Arg\text{-}1^+$ and $MHCII^+$ cells ± SEM. Significant appearance of MHCII, Arg-1 and MHCII/Arg-1 expression is indicated by the *, # and ◊ symbols, respectively. */#/◊ P<0.05, **P<0.01, One sample t-test (n= 3–6 mice).

Figure 6: LV mediated expression of IL-13 in the splenium induces a unique phenotypic and cytokine profile during cuprizone treatment.

Graphs show the mRNA expression of cytokines and phenotypic markers at the level of the CC after injection of LV followed by four weeks of cuprizone supplemented diet for (a) Arg-1, Arginase-1; (b) YM-1, chitinase-like 3; (c) Gal-3, galectin-3; (d) TNF-α, tumor necrosis factor α; (e) IL-1β, interleukin 1β; (f) iNOS, inducible nitric oxide synthase. Values are expressed as fold versus control (No inj. CONTROL) ± SEM. *P<0.05, **P<0.01, ***P<0.001, One-way ANOVA, Dunnett's multiple comparison test (n= 7-10 mice).

Figure 7: Both microglia and macrophage phenotype is modulated through LV mediated expression of IL-13 in the splenium.

(a) $eGFP^+$ bone marrow chimeric mice were generated in order to differentiate infiltrating macrophages (green) from brain-resident microglia. At eight week of age mice received an injection of BFP LV, IL-13 LV or no injection (No inj.) and were fed a cuprizone diet for a period of four weeks to induce inflammation and demyelination. (b) Representative T_2-weighted images show hyper-intense contrast at the level of the splenium of the CC indicative of neuro-inflammation and demyelination following four weeks of cuprizone diet, but not in the case of mice that also received the IL-13 LV injection (Arrow indicates the site of injection of IL-13 LV and associated protection against cuprizone). (c) Representative images of each experimental group stained for MHCII (blue) and Arg-1 (red). Scale bar = 100 µm. (d) Graph shows the mean density ± RMSD (root mean square deviation) of $eGFP^+$ infiltrating macrophages into the splenium. *P<0.05, Generalized estimating equations and Bonferroni post hoc test (n = 3 mice). (d) Graph shows the mean density ± RMSD of Arg-1 and MHCII cells. Significant appearance of $MHCII^+$, $Arg\text{-}1^+$ and $MHCII/Arg\text{-}1^+$ expressing cells is indicated by the *, # and ◊ symbols, respectively. */#/◊ P<0.05, **P<0.01, ◊◊◊P<0.001, Generalized estimating equation, FDR corrected (n = 3 mice).

Figure 8: Therapeutic LV mediated expression of IL-13 in the splenium protects against severe cuprizone-induced demyelination and is associated with an altered microglia/macrophage phenotype.

(a) Eight week old mice were assigned to a control or cuprizone treated group. In order to test whether IL-13 LV injection may exert its protective effect during cuprizone-induced CNS neuro-inflammation and demyelination, a subgroup of mice that received the cuprizone diet for a period of 2.5 weeks were injected with the IL-13 LV. Magnetic resonance imaging evaluation and histological analysis were performed after 4 weeks of cuprizone administration. (b) T_2 values of individual mice are displayed in the graph with mean ± SD and reveal a significant increase of the normal T_2 for IL-13 LV injected cuprizone treated mice (n = 5-15 mice). **P<0.01, ***P<0.001, Wilcoxon rank sum test, FDR corrected (n = 5-15 mice). (c) MTR of individuals are displayed in the graph with mean ± SD and reveal a lower deviation of the normal MTR of IL-13 LV injected cuprizone treated mice (n = 5-15 mice). **P<0.01, ***P<0.001, Wilcoxon rank sum test, FDR corrected (n = 5-15 mice). (d) Histological analyses performed at the level of the splenium in mice that received the IL-13 LV injection after 2.5 weeks of cuprizone diet. Representative images showing the presence of F4/80$^+$ inflammatory cells (red), the MHCII/Arg-1 phenotypic properties of inflammatory cells (green and red, respectively), the presence of astrogliosis (GFAP, red) the presence of myelin (MBP, red) and the presence of CC1+ oligodendrocytes (red). (n = 5-8 mice analyzed per group). Scale bar = 100 µm. Quantitative analysis confirming significantly reduced F4/80$^+$ inflammatory responses (e), alternative activation of microglia/macrophages (f), reduced astrogliosis (g), reduced demyelination (h) and oligodendrocyte survival (i) at the level of the splenium in mice that received the IL-13 LV injection after 2.5 weeks of cuprizone diet. Graphs e, g, h and I display mean +/- SD, *P<0.05, ***P<0.001, One-way ANOVA and Tukey post hoc test (n = 5 - 8 mice). Graph (f) displays mean +/- SD for the density of Arg-1$^+$ and MHCII$^+$ cells. Significant appearance of Arg-1 and MHCII/Arg-1 expression is indicated by the # and ◊ symbols, respectively. ## P<0.01, ◊◊◊P<0.001, One sample t-test (n= 5–8 mice).

FIGURE 1

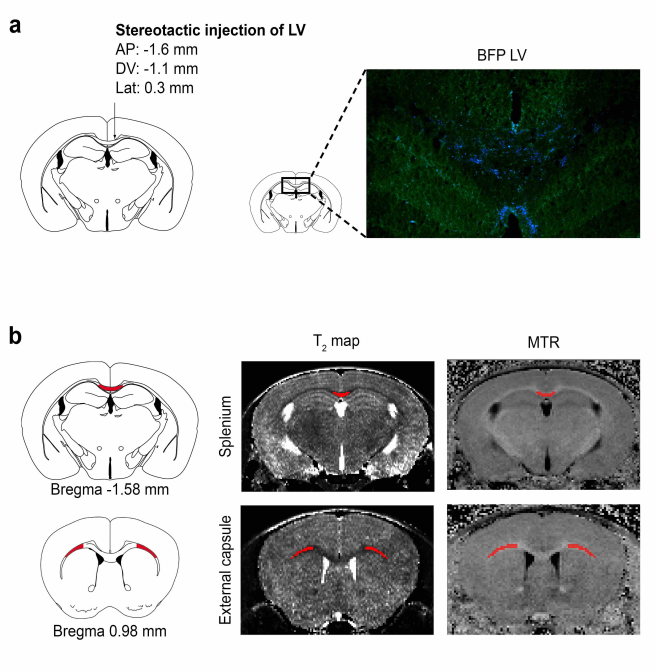
a
Stereotactic injection of LV
AP: -1.6 mm
DV: -1.1 mm
Lat: 0.3 mm
BFP LV
b
T2 map
MTR
Splenium
External capsule
Bregma -1.58 mm
Bregma 0.98 mm

FIGURE 2

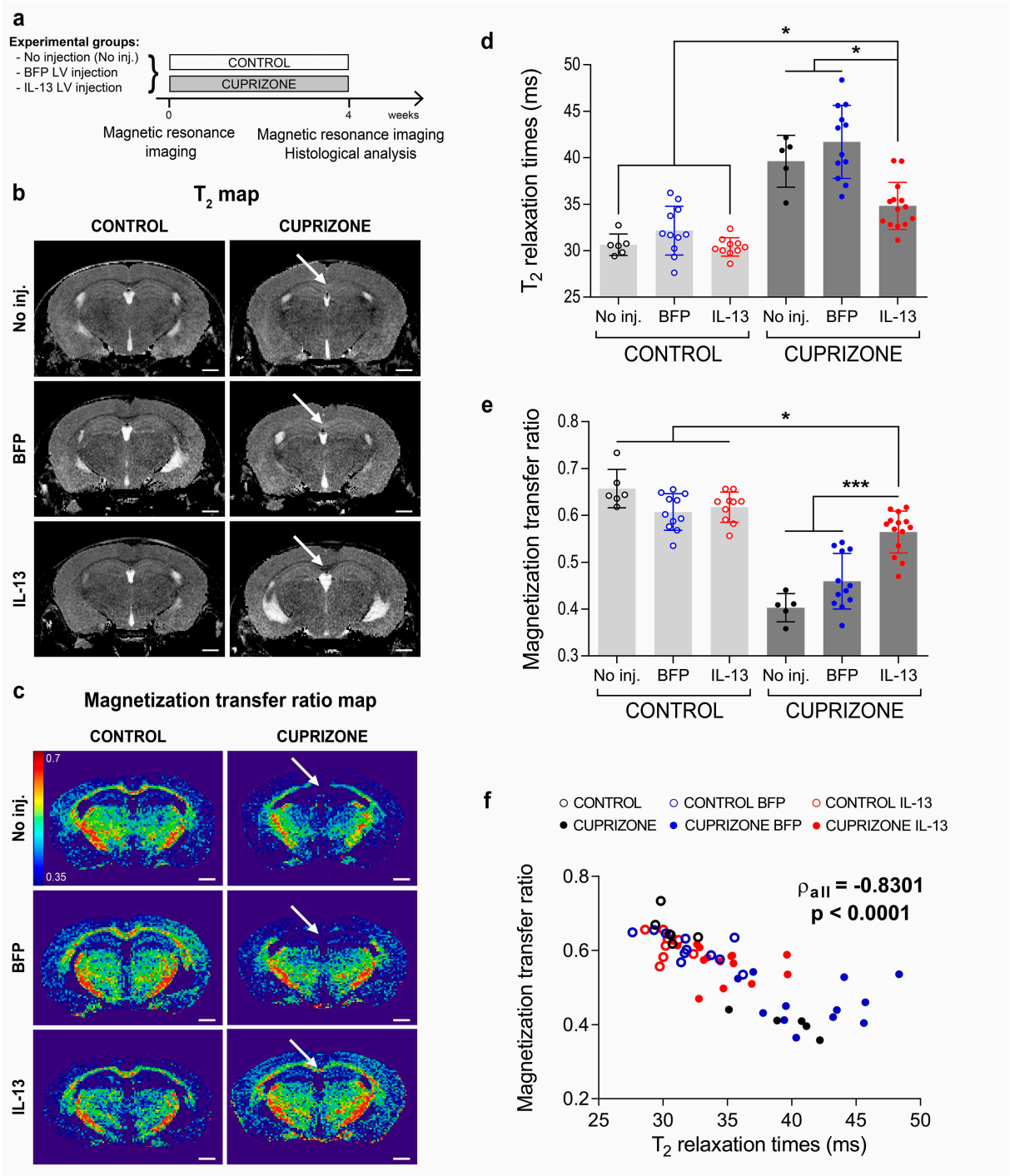
a
Experimental groups:
- No injection (No inj.)
- BFP LV injection
- IL-13 LV injection
CONTROL
CUPRIZONE
0
4
weeks
Magnetic resonance imaging
Magnetic resonance imaging
Histological analysis
b
T2 map
CONTROL
CUPRIZONE
No inj.
BFP
IL-13
c
Magnetization transfer ratio map
CONTROL
CUPRIZONE
0.7
0.35
No inj.
BFP
IL-13
d
T2 relaxation times (ms)
50
45
40
35
30
25
*
*
No inj.
BFP
IL-13
No inj.
BFP
IL-13
CONTROL
CUPRIZONE
e
Magnetization transfer ratio
0.8
0.7
0.6
0.5
0.4
0.3
*
***
No inj.
BFP
IL-13
No inj.
BFP
IL-13
CONTROL
CUPRIZONE
f
CONTROL
CONTROL BFP
CONTROL IL-13
CUPRIZONE
CUPRIZONE BFP
CUPRIZONE IL-13
Magnetization transfer ratio
0.8
0.6
0.4
0.2
ρall = -0.8301
p < 0.0001
25
30
35
40
45
50
T2 relaxation times (ms)

FIGURE 3

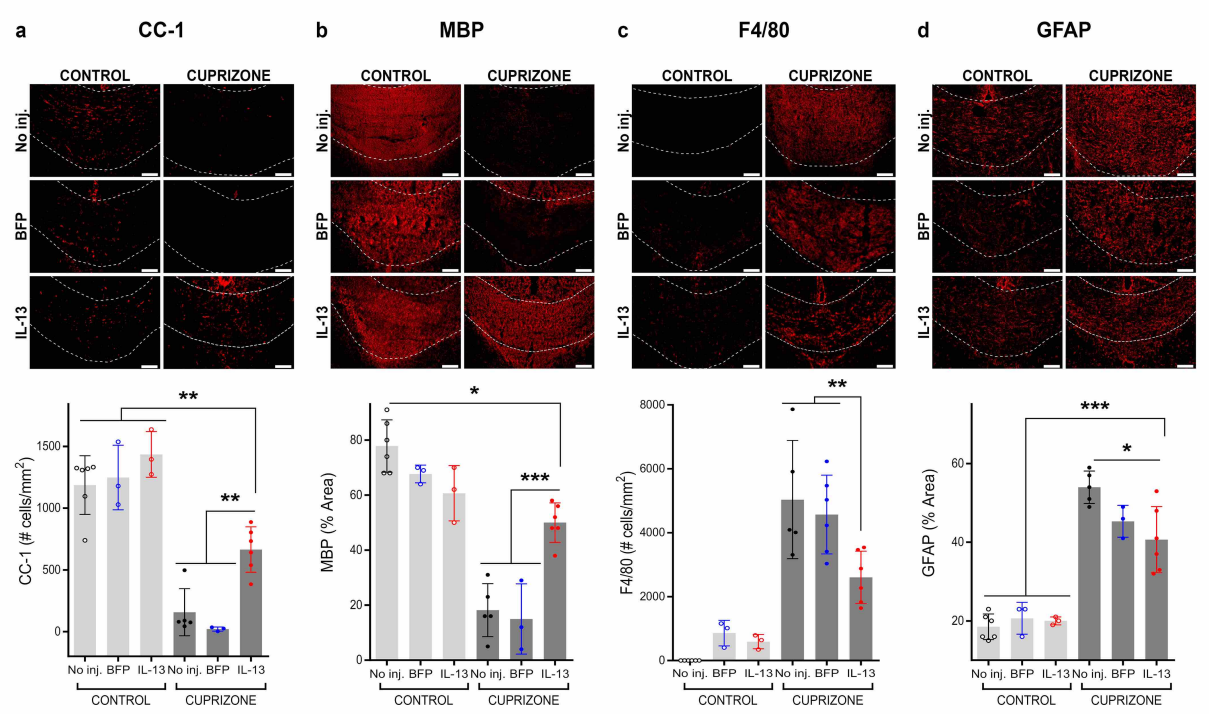
a
CC-1
b
MBP
c
F4/80
d
GFAP
CONTROL
CUPRIZONE
No inj.
BFP
IL-13
CC-1 (# cells/mm2)
MBP (% Area)
F4/80 (# cells/mm2)
GFAP (% Area)
No inj. BFP IL-13 No inj. BFP IL-13
CONTROL
CUPRIZONE

FIGURE 4

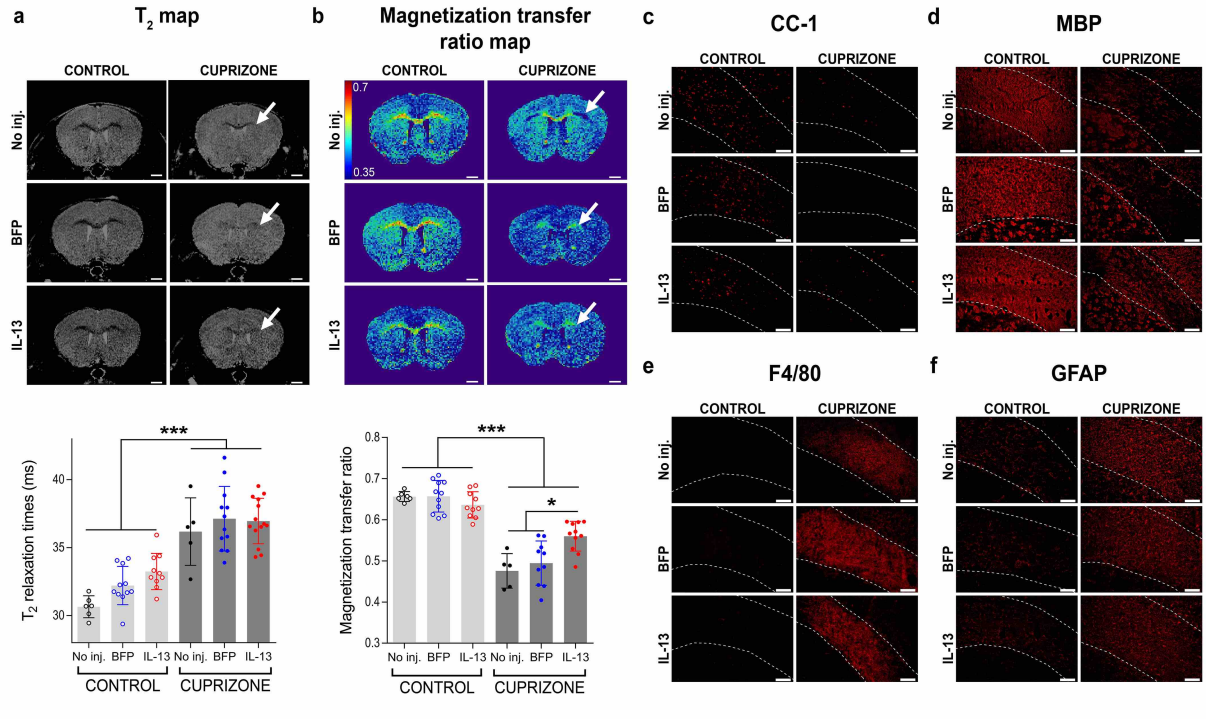
a
T2 map
b
Magnetization transfer ratio map
c
CC-1
d
MBP
e
F4/80
f
GFAP
CONTROL
CUPRIZONE
No inj.
BFP
IL-13
0.7
0.35
T2 relaxation times (ms)
Magnetization transfer ratio
***
*
No inj. BFP IL-13 No inj. BFP IL-13
CONTROL
CUPRIZONE

FIGURE 5

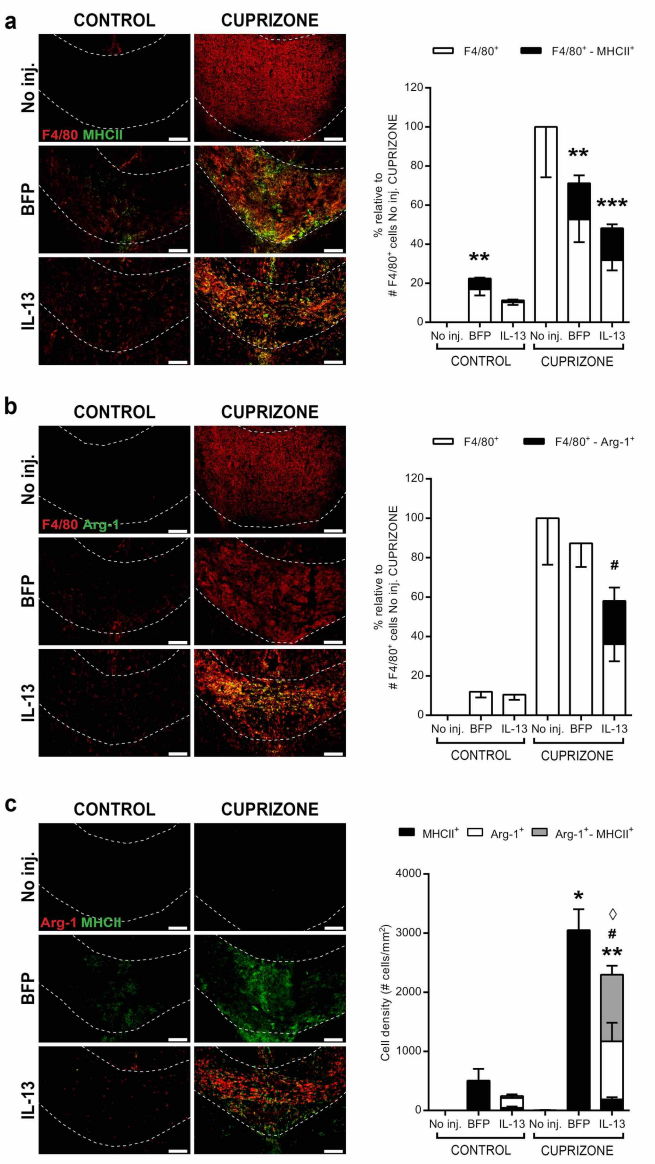
a
CONTROL
CUPRIZONE
No inj.
BFP
IL-13
F4/80 MHCII
F4/80+
F4/80+ - MHCII+
% relative to # F4/80+ cells No inj. CUPRIZONE
No inj. BFP IL-13 No inj. BFP IL-13
CONTROL
CUPRIZONE
b
F4/80 Arg-1
F4/80+ - Arg-1+
c
Arg-1 MHCII
MHCII+
Arg-1+
Arg-1+- MHCII+
Cell density (# cells/mm2)

FIGURE 6

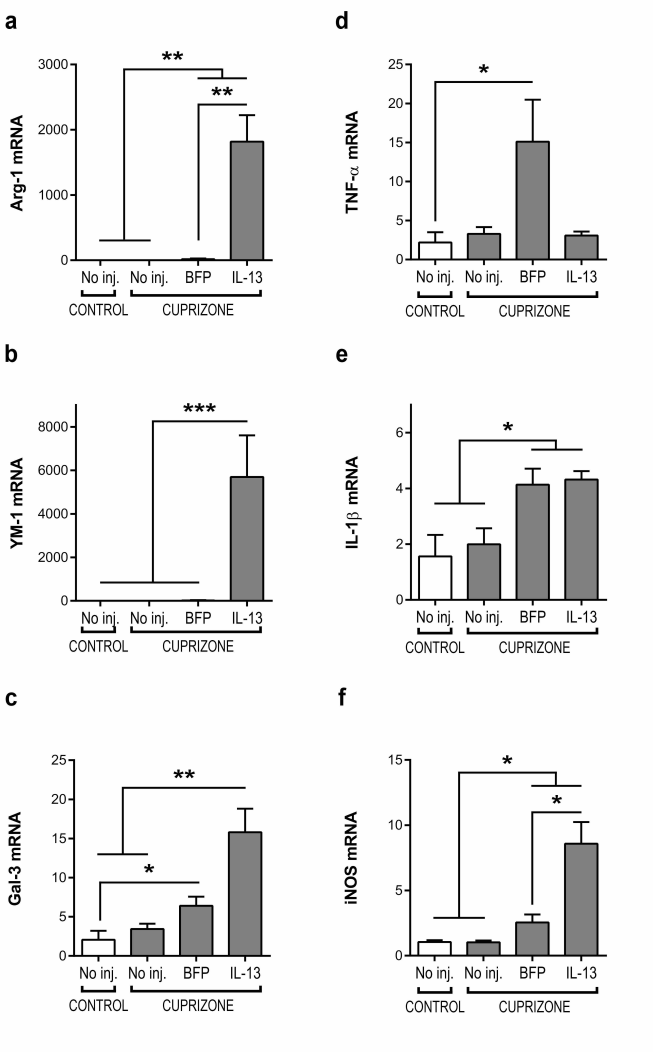
a
Arg-1 mRNA
3000
2000
1000
0
**
**
No inj.
No inj.
BFP
IL-13
CONTROL
CUPRIZONE
d
TNF-α mRNA
25
20
15
10
5
0
*
No inj.
No inj.
BFP
IL-13
CONTROL
CUPRIZONE
b
YM-1 mRNA
8000
6000
4000
2000
0
***
No inj.
No inj.
BFP
IL-13
CONTROL
CUPRIZONE
e
IL-1β mRNA
6
4
2
0
*
No inj.
No inj.
BFP
IL-13
CONTROL
CUPRIZONE
c
Gal-3 mRNA
25
20
15
10
5
0
**
*
No inj.
No inj.
BFP
IL-13
CONTROL
CUPRIZONE
f
iNOS mRNA
15
10
5
0
*
*
No inj.
No inj.
BFP
IL-13
CONTROL
CUPRIZONE

FIGURE 7

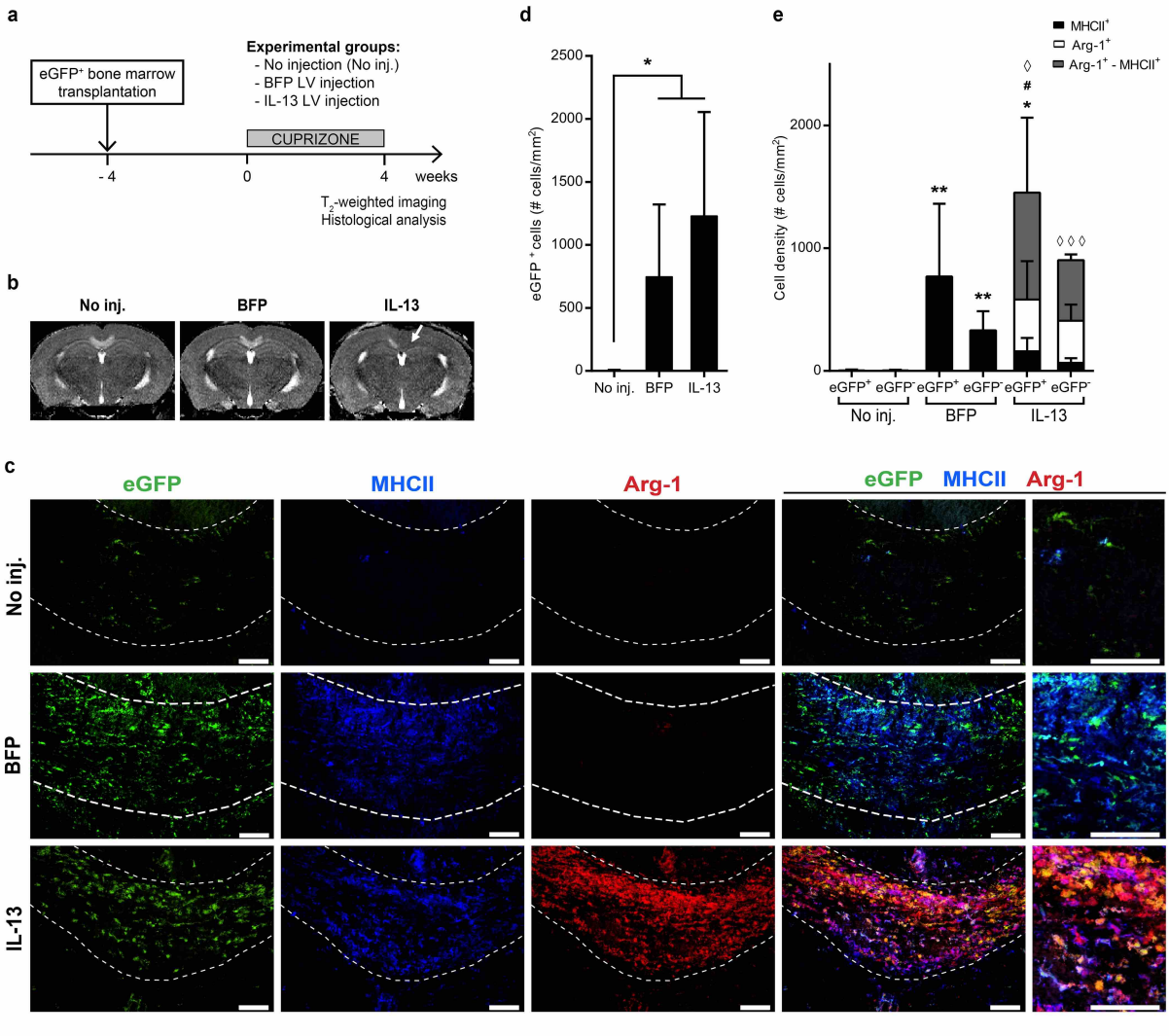
a
eGFP+ bone marrow transplantation
Experimental groups:
- No injection (No inj.)
- BFP LV injection
- IL-13 LV injection
CUPRIZONE
- 4
0
4
weeks
T2-weighted imaging
Histological analysis
b
No inj.
BFP
IL-13
d
eGFP + cells (# cells/mm2)
2500
2000
1500
1000
500
0
No inj.
BFP
IL-13
e
MHCII+
Arg-1+
Arg-1+ - MHCII+
Cell density (# cells/mm2)
2000
1000
0
eGFP+ eGFP- eGFP+ eGFP- eGFP+ eGFP-
No inj.
BFP
IL-13
c
eGFP
MHCII
Arg-1
eGFP MHCII Arg-1
No inj.
BFP
IL-13

FIGURE 8

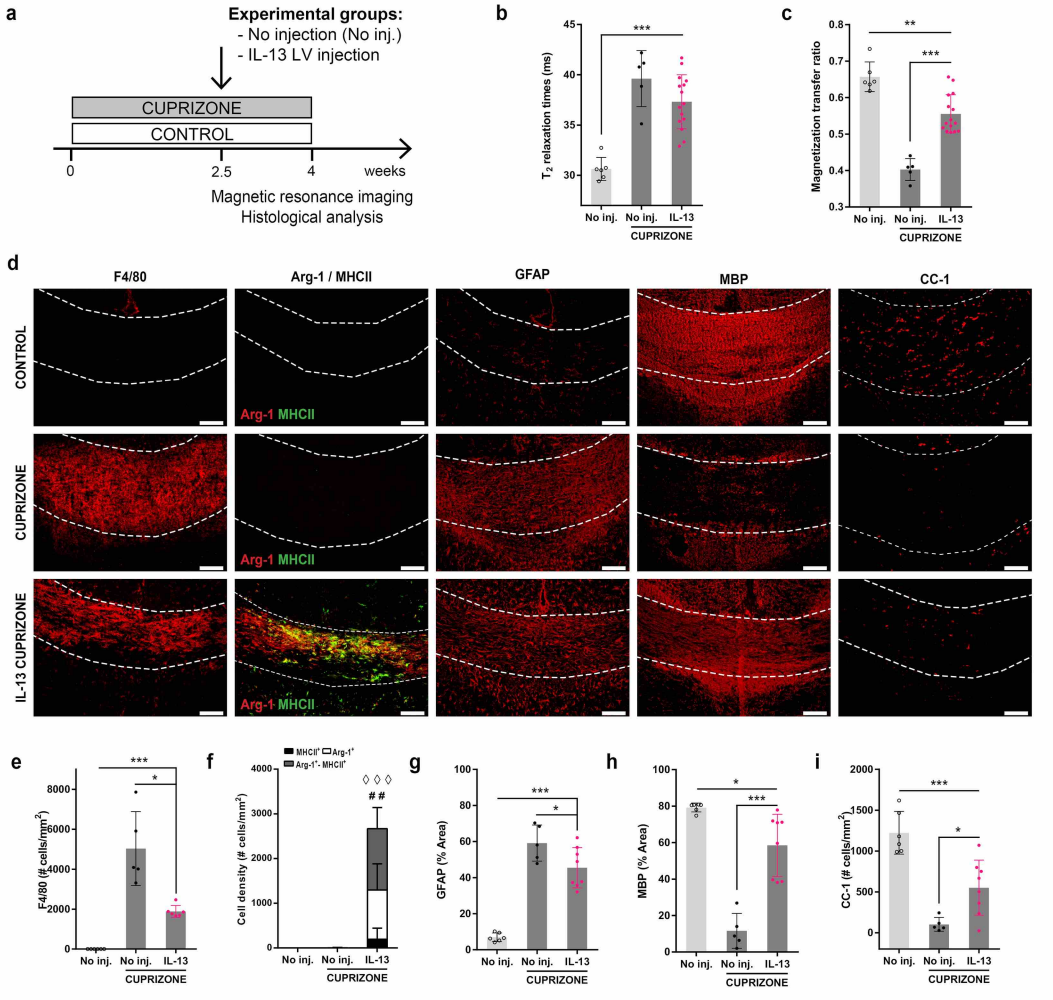
a
Experimental groups:
- No injection (No inj.)
- IL-13 LV injection
CUPRIZONE
CONTROL
0
2.5
4
weeks
Magnetic resonance imaging
Histological analysis
b
T2 relaxation times (ms)
No inj.
No inj.
IL-13
CUPRIZONE
c
Magnetization transfer ratio
d
F4/80
Arg-1 / MHCII
GFAP
MBP
CC-1
CONTROL
CUPRIZONE
IL-13 CUPRIZONE
Arg-1 MHCII
e
F4/80 (# cells/mm2)
f
Cell density (# cells/mm2)
MHCII+ Arg-1+
Arg-1+ MHCII+
g
GFAP (% Area)
h
MBP (% Area)
i
CC-1 (# cells/mm2)

SUPPLEMENTARY FIGURE S1

Correlation analyses of MRI and histological metrics at the level of the splenium.

Scatter plots show significant correlations of T_2 values (a-d) or MTR (e-h) with oligodendrocytes (CC-1), myelination (MBP), activated microglia/macrophages (F4/80) and astrocytes (GFAP).

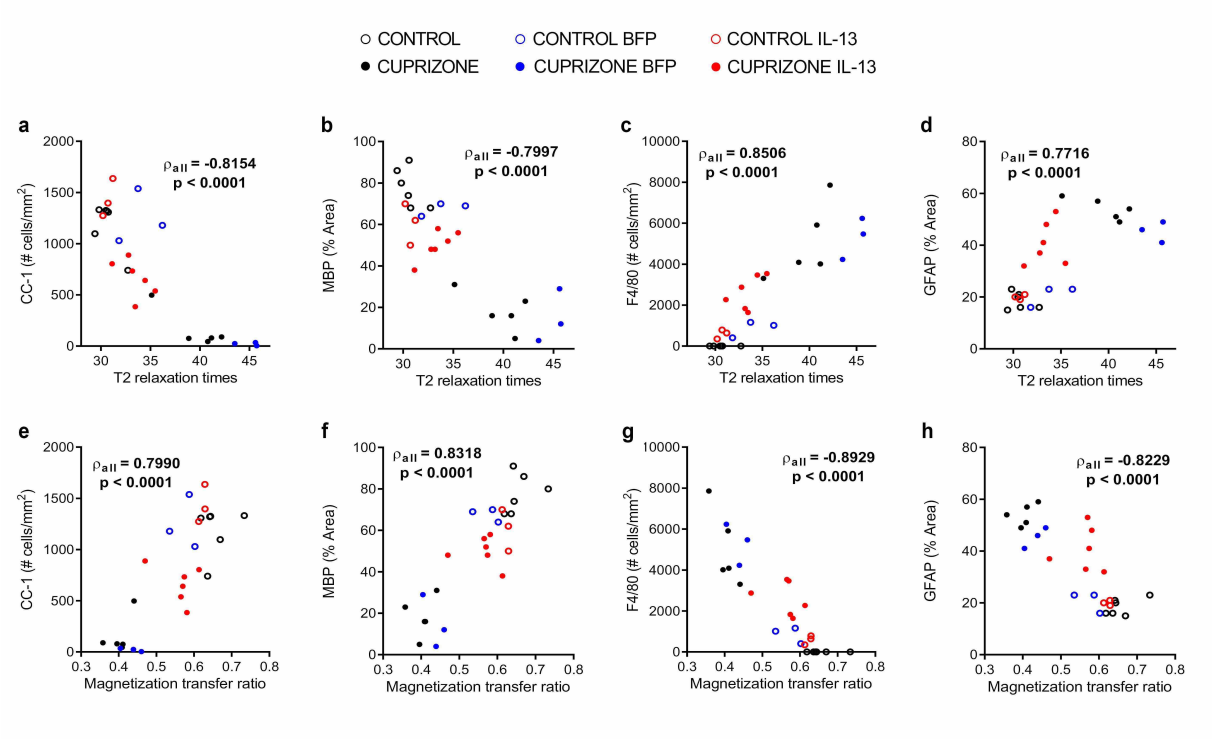

SUPPLEMENTARY FIGURE S2

Correlation analyses of MRI and histological metrics at the level of the external capsule.

Scatter plots show significant correlations of T_2 values with MTR (a), T_2 values (b, c and d) or MTR (e, f and g) with oligodendrocytes (CC-1), activated microglia/macrophages (F4/80) and astrocytes (GFAP).

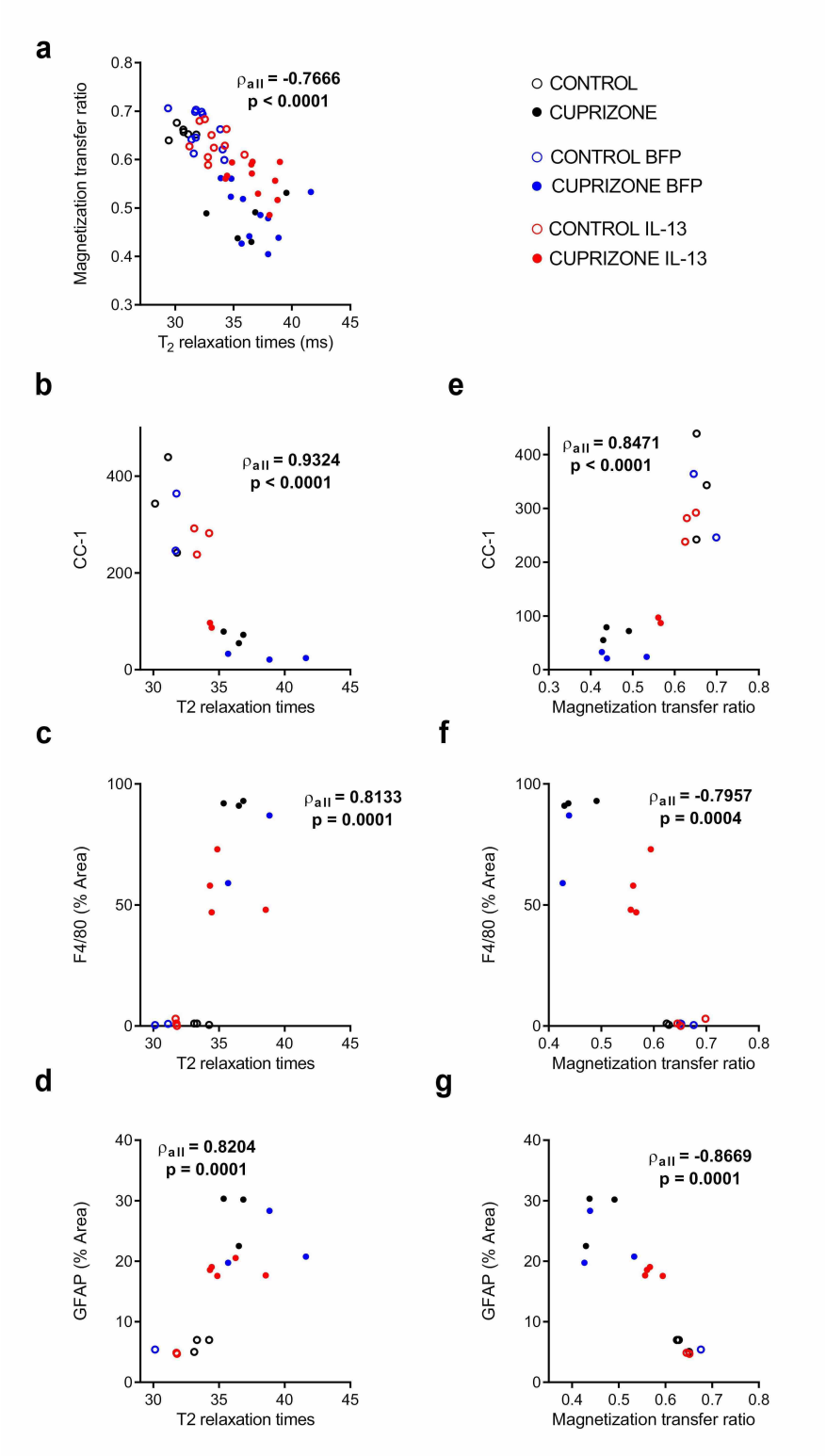

SUPPLEMENTARY FIGURE S3

MRI evaluation of cuprizone treated mice following LV mediated expression of IL-4.

(a) To induce inflammation and demyelination, mice were fed a cuprizone supplemented diet for a period of four weeks, while mice of the control groups were fed a regular rodent chow. On the first day of cuprizone administration mice received an injection of IL-4 LV or no injection (No inj.) and were assigned to a cuprizone or control group. MRI was performed after four weeks of cuprizone feeding, immediately followed by immunofluorescence analysis. (b) Left panel shows representative T_2 maps, while right panel shows representative color-coded MTR images, for mice that received the IL-4 LV injection and assigned to the control or cuprizone treated group at the level of the splenium of the CC. All scale bars indicate 1 mm. T_2 value of individual mice are displayed in the graph with mean ± SEM and reveal a lower deviation of the normal T_2 of IL-4 LV injected cuprizone treated mice (n = 5-9 mice). **P<0.01, One-way Anova, Tukey post hoc test. All significance are indicated in supplementary table 16. (e) Similarly, MTR of individual mice are displayed in the graph with mean ± SD and indicate a lower deviation of the MTR of IL-14 LV injected cuprizone treated mice (n = 5-9 mice). *P<0.05, ***P<0.001, One-way Anova, Tukey post hoc test. All significance are indicated in supplementary table 16. (c) Representative images taken at the level of the splenium of the CC show myelin preservation in cuprizone treated mice that received the IL-4 LV injection (MBP, red), as well as the presence of Arg-1 expressing cells (Arg-1, red), (n = 3 mice analyzed per group). Scale bar = 100 µm.

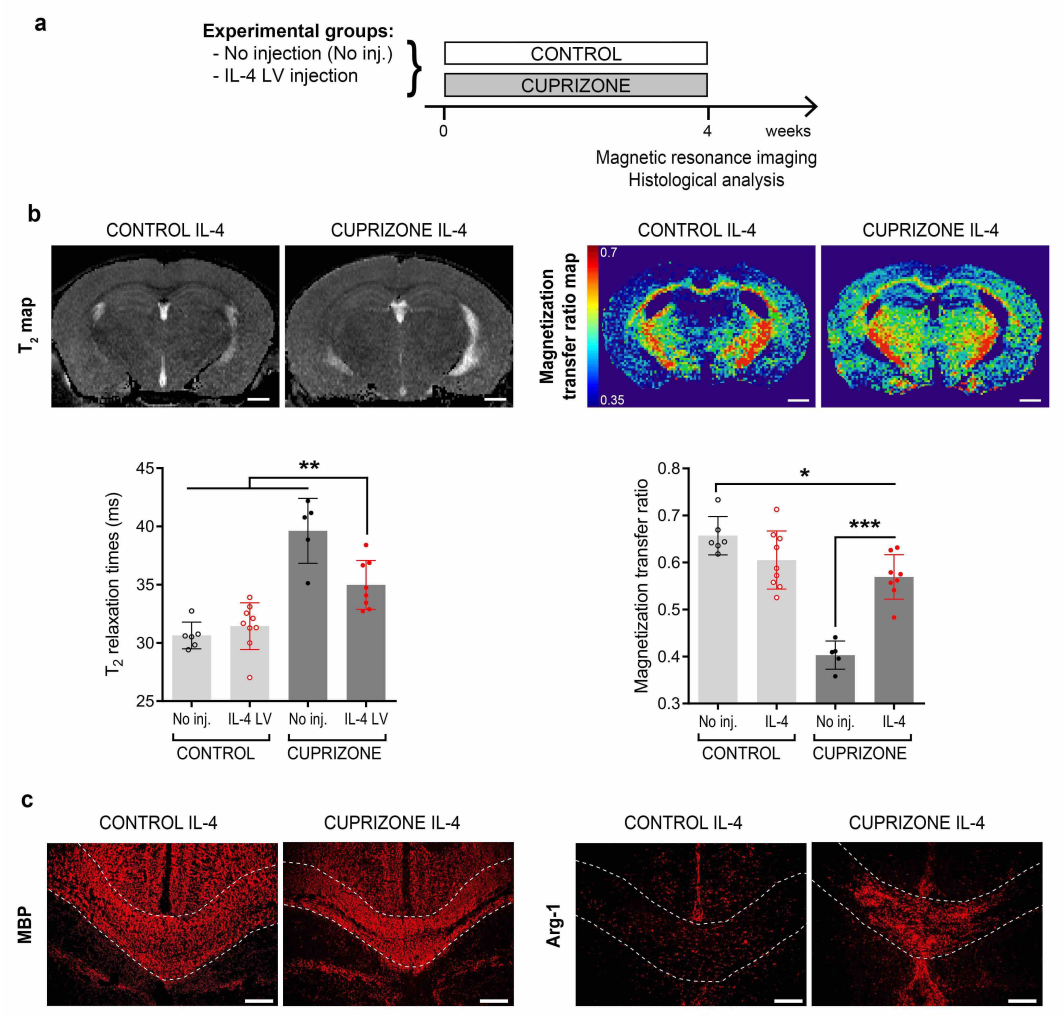

SUPPLEMENTARY TABLE S1

PCR primers used to obtain data presented in figure 6.

Primer	Mouse Sequence	Accession nº	Amplicon length	Region
ARG1	F: AGGGTTACGGCCGGTGGAGAG R: CCTCAGTGCTGCAGGGCCTTT	NM_007482.3	173	Exon 5 Exon 7
GAL3	F: GCCCTTGCCTGGAGGAGTCATG R: CATTGAAGCGGGGGTTAAAGTGG	NM_010705.3	134	Exon 4 Exon 5
IL1b	F: GAAGAGCCCATCCTCTGTGA R: TTCATCTCGGAGCCTGTAGTG	NM_008361.4	96	Exon 4/5 Exon 5
iNOS	F: CAGCTGGGCTGTACAAACCTT R: CATTGGAAGTGAAGCGTTTCG	XM_006532446.2	95	Exon 17 Exon 18
SDHA	F: TGGGGAGTGCCGTGGTGTCA R: CATGGCTGTGCCGTCCCCTG	NM_023281.1	154	Exon 6 Exon 7
TGFB1	F: TGCTTCAGCTCCACAGAGAA R: TACTGTGTGTCCAGGCTCCA	NM_011577.1	155	Exon 5/6 Exon 6
TNFA2	F: GGGGCCACCACGCTCTTCTGTC R: TGGGCTACGGGCTTGTCACTCG	NM_013693.3	155	Exon 1 Exon 3
YM1	F: CAGGTCTGGCAATTCTTCTGAA R: GTCTTGCTCATGTGTGTAAGTGA	NM_145126.2	197	Exon 1/2 Exon 3